Magnetic Signatures of the January 15 2022 Hunga Tonga–Hunga Haʻapai Volcanic Eruption

Neesha Schnepf[1], Takuto Minami[2], Hiroaki Toh[3], and Manoj Nair[4]

[1]Laboratory for Atmospheric & Space Physics
[2]Kobe University
[3]Kyoto University
[4]Cooperative Institute for Research in Environmental Sciences

November 26, 2022

Abstract

On January 15, 2022, at around 04:00 UTC, the submarine volcano Hunga Tonga-Hunga Haʻapai explosively erupted. We examine data from ten Pacific Ocean geomagnetic observatories and process the data using both high pass filters and cross-wavelet analyses to enable evaluating the time-frequency characteristics of the magnetic signals across the Pacific region. At the Western Samoa observatory (API), magnetic signals of 3-8 minutes period, and ~1nT amplitudes, arrived at ~04:44 UTC. API's signals are likely due to ionospheric sources. The observatories at Chichijima Island (CBI) and Easter Island (IPM) both had local magnetic signatures concurrent with the eruption's water wave arrival and period ranges from, respectively, 13-93 minutes and 5-100+ minutes. At CBI and IPM, the magnetic signal may be due to both the eruption's tsunami water wave and atmospheric/ionospheric sources. Our results suggest that the magnetic signatures from the eruption are identifiable and may be further separated in future studies.

Magnetic Signatures of the January 15 2022 Hunga Tonga–Hunga Ha'apai Volcanic Eruption

N. R. Schnepf[1], T. Minami[2], H. Toh[3], and M. C. Nair[4,5]

[1]University of Colorado Boulder, Laboratory for Atmospheric and Space Physics, Boulder, 80305, USA
[2]Kobe University, Department of Planetology, Kobe, 657-8501, Japan
[3]Kyoto University, Data Analysis Centre for Geomagnetism and Space Magnetism, Kyoto, 606-8502, Japan
[4]University of Colorado Boulder, Cooperative Institute for Research in Environmental Sciences, Boulder, 80305, USA
[5]National Oceanic and Atmospheric Administration, National Centers for Environmental Information, Boulder, 80305, USA

Key Points:

- Magnetic signals of 3-8 minutes period arrived at Western Samoa (API) and are likely due to ionospheric sources.
- Both Chichijima Island (CBI) and Easter Island (IPM) had local magnetic signatures concurrent with the eruption's water wave arrival.
- The CBI and IPM magnetic signals' may be due to both the eruption's tsunami water wave and atmospheric/ionospheric waves.

Corresponding author: Neesha R. Schnepf, neesha.schnepf@lasp.colorado.edu

Abstract

On January 15, 2022, at around 04:00 UTC, the submarine volcano Hunga Tonga-Hunga Ha'apai explosively erupted. We examine data from ten Pacific Ocean geomagnetic observatories and process the data using both high pass filters and cross-wavelet analyses to enable evaluating the time-frequency characteristics of the magnetic signals across the Pacific region. At the Western Samoa observatory (API), magnetic signals of 3-8 minutes period, and ∼1nT amplitudes, arrived at ∼04:44 UTC. API's signals are likely due to ionospheric sources. The observatories at Chichijima Island (CBI) and Easter Island (IPM) both had local magnetic signatures concurrent with the eruption's water wave arrival and period ranges from, respectively, 13-93 minutes and 5-100+ minutes. At CBI and IPM, the magnetic signal may be due to both the eruption's tsunami water wave and atmospheric/ionospheric sources. Our results suggest that the magnetic signatures from the eruption are identifiable and may be further separated in future studies.

Plain Language Summary

On January 15, 2022, at around 04:00 UTC, the submarine volcano Hunga Tonga-Hunga Ha'apai erupted in a violent explosion. Previous studies have identified magnetic signals from earthquake-created tsunamis, however, no such studies have identified marine magnetic signals from eruption-created tsunamis. Identifying tsunami magnetic signals may enable improving tsunami warning systems. Towards this aim, we examine data from ten Pacific Ocean geomagnetic observatories. We processed the data using mathematical methods that enable examining the different wave components of the timeseries. We find magnetic signals likely caused by the eruption at three different Pacific island observatories (API- Western Samoa, CBI- Chichijima Island, and IPM- Easter Island).

1 Introduction

On January 15, 2022, at around 04:00 UTC, the submarine volcano Hunga Tonga-Hunga Ha'apai explosively erupted. The volcano had been erupting for the previous 24 hours, as well as intermittently in the preceding month, but the explosion that started at 04:00 UTC on Jan. 15 was by far the largest event. According to seismic data, the eruption itself lasted about ten minutes (Tiampo, n.d.). The shock wave from the largest explosion of the eruption produced a sonic boom that was heard within 9 hours in Alaska, USA (9,370 km away). Tonga's islands were bombarded by tsunami waves of 2-15m height and three Tongan people died from the tsunami so far, while many others were injured. The tsunami caused flooding, property damage, and two deaths as far away as Peru (Sennert, 2022).

Since the foundational work of Faraday (1832), physicists have known that salty water traveling through Earth's background magnetic field induces electric currents and secondary electromagnetic fields. Recently, there has been much work to study and characterize the magnetic signals from earthquake induced tsunamis (Manoj et al., 2011; Toh et al., 2011; Utada et al., 2011; Ichihara et al., 2013; Sugioka et al., 2014; Tatehata et al., 2015; Klausner et al., 2016; Schnepf et al., 2016; Minami et al., 2017, 2021; Lin et al., 2021). There are no past studies of the marine electromagnetic signals induced by volcanic eruptions. Instead, there is much literature on volcanic eruptions' atmospheric and ionospheric impacts to the point that ionospheric data has been used to provide information on the volcanic eruption (Astafyeva, 2019; Heki, 2006; Dautermann, Calais, Lognonné, & Mattioli, 2009; Dautermann, Calais, & Mattioli, 2009; Nakashima et al., 2016; Shults et al., 2016; Liu et al., 2017). As shown by Kubota et al. (2022), the Hunga Tonga-Hunga Ha'apai eruption's atmospheric acoustic waves deformed the sea surface so that tsunami-like water level variations occurred hours before the actual tsunami water wave arrived. Undoubtedly, these acoustic waves also caused ionospheric disturbances.

Table 1. Location of the selected geomagnetic observatories. Note: * The nearest water level station to API was located ∼128 km southeast of the geomagnetic observatory and † marks the observatory used as the remote reference in the cross-wavelet analysis. The volcanic eruption occurred at 184.618°E and 20.536°S.

Observatory	Location	Latitude (°N)	Longitude (°E)	Altitude (m)	Nearest Distance to Shore (km)	Distance to Eruption (km)	Water Wave Arrival (UTC)
API	Western Samoa	-13.807	188.225	2	0	837.6	05:12*
ASP†	Australia	–23.762	133.883	557	>900	5218.7	
CBI	Japan	27.096	142.185	155	0.2	6978.2	11:11
CNB	Australia	-35.320	149.360	859	101	3810.2	
CTA	Australia	-20.090	146.264	370	108	3996.6	
EYR	New Zealand	-43.474	172.393	102	26.3	2786.4	
HON	United States	21.320	202.000	4	0.9	5001.5	09:07
IPM	Easter Island	-27.171	250.580	83	1.6	6685.6	13:42
KAK	Japan	36.232	140.186	36	34	7831.5	
KNY	Japan	31.420	130.880	107	10.8	8120	
MMB	Japan	43.910	144.190	42	11.8	8240.6	
PPT	Tahiti	-17.567	210.426	357	2.5	2733.5	06:48

Here we provide a comprehensive evaluation of magnetic signatures from the 04:00 January 15 2022 Hunga Tonga–Hunga Ha‘apai volcanic eruption. We do not attempt to separate internal and external magnetic fields– the ”event signal” may be from the magnetic fields induced by the tsunami water wave, by the propagation of acoustic waves in the neutral atmosphere (which then deformed the electrically conductive sea surface) or in the electrically conductive ionosphere (which directly induces its own magnetic field) (Astafyeva, 2019; Kubota et al., 2022). Instead, we analyze the time-frequency characteristics of signals at several Pacific Ocean observatories to determine whether magnetic signals are local to a given observatory or concurrent at multiple.

2 Analysis of Observatory Data

2.1 Observatory data

Data was obtained from several International Real-time Magnetic Observatory Network (INTERMAGNET) observatories and also from a Japan Meteorological Agency (JMA) observatory (CBI) located at Chichijima Island. Table 1 specifies the locations of these observatories and Figure 1 illustrates their positions relative to the eruption site (denoted by a red star).

For each of these observatories, vector data of 1 minute sampling was used. The downward vertical component (Z) was used as is, but the northward (X) and eastward (Y) components were combined into one horizontal component ($H = \sqrt{X^2 + Y^2}$).

We used observatories from a variety of locations in the Pacific Ocean. As seen in Table 1, API (Western Samoa), CBI (Chichijima Island, Japan), and HON (Honolulu, USA) were the three observatories with the closest proximity to seawater, with API having the best signal-to-noise ratio of any of the observatories since it is directly on the coast (Supplementary Figure S2). The Chichijima station is about 200 m from the beach, however, it is at an undisturbed portion of the island. This especially contrasts with the Honolulu observatory: HON is under 1 km from seawater but between the observatory and beach are neighborhoods that likely cause significant anthropogenic noise (Supplementary Figure S3).

Closely following these three observatories, IPM (Easter Island, Chile) and PPT (Tahiti, French Polynesia) are the next two observatories closest to seawater. Similar to CBI, the Easter Island observatory is in an undisturbed portion of the island, albeit further from the coast (1.6 km versus 200 m, Supplementary Figure S4). Meanwhile the PPT observatory has challenges similar to HON: it is 2.5 km inland (versus HON's 900 m) and at 357 m elevation (unlike HON's 4m altitude) with urban electromagnetic signals resting between it and the sea (Supplementary Figure S5).

For these five island stations we obtained water wave height variation data. As discussed in the following section, the wave height data was used to determine when the eruption's water wave (due to either the atmospheric shock wave or the oceanic tsunami wave) reached the observatory. Note that for Western Samoa (API), the water level data was $\sim$128km away from API on a different island. Supplementary Figure S2 shows their locations. Neither observatory directly faces the eruption and the water level station is in an east-facing bay that is $\sim$15 km further from the eruption than API. This further complicates the time lag between the water wave arrival at the geomagnetic observatory versus at the water level station.

The observatories CNB (Canberra, Australia), CTA (Charter Towers, Australia), EYR (Eyrewell, New Zealand), KAK (Kakioka, Japan), KNY (Kanoya, Japan), and MMB (Memambetsu, Japan) were selected for evaluating what time-frequency magnetic field characteristics were similar across the wider region. The observatory ASP (Alice Springs, Australia) was selected to be a remote reference station for the cross-wavelet analysis (discussed in section 2.3) since it is deep in the Australian desert. The raw data from all of these stations are shown in Supplementary Figures S9-S20.

2.2 Removing longer period signals via high-pass filtering

The dominant variability in water level data is that due to tides. Variation in geomagnetic data is dominated by the daily fluctuations of the ionosphere– many of which are also solar synchronous. For both data sets, similar to the method of Schnepf et al. (2016), the data underwent a high pass butterworth filter. Schnepf et al. (2016), Toh et al. (2011), Manoj et al. (2011), and Utada et al. (2011) all found that tsunami magnetic signals had periods typically within 10-30 minutes. Ionospheric disturbances due to volcanic eruptions have been identified to have signals within a period range of 208.3 s to 1000 s (frequencies of 1-4.8 mHz) (Astafyeva, 2019; Dautermann, Calais, & Mattioli, 2009; Nakashima et al., 2016). Thus, we used a maximum period of 30 minutes so that signals with periodicities of 30 min or greater were removed. The results of this high pass filter are shown in Figures 2, 3, and 4 for the observatories at, respectively, Western Samoa (API), Chichijima (CBI), and Easter Island (IPM).

The aforementioned tsunami studies were focused on those created by earthquakes. Because the volcanic eruption was a less impulsive and less discrete initiating event as compared to an earthquake, we also examined the data using a maximum period of 120 minutes. These results are also shown in Figures 2 - 4.

To determine when the eruption's water wave reached each observatory, the start of water wave height variations was selected for both sets of high pass filtered data. Note that this arriving water wave likely show that the atmospheric shock waves caused per-

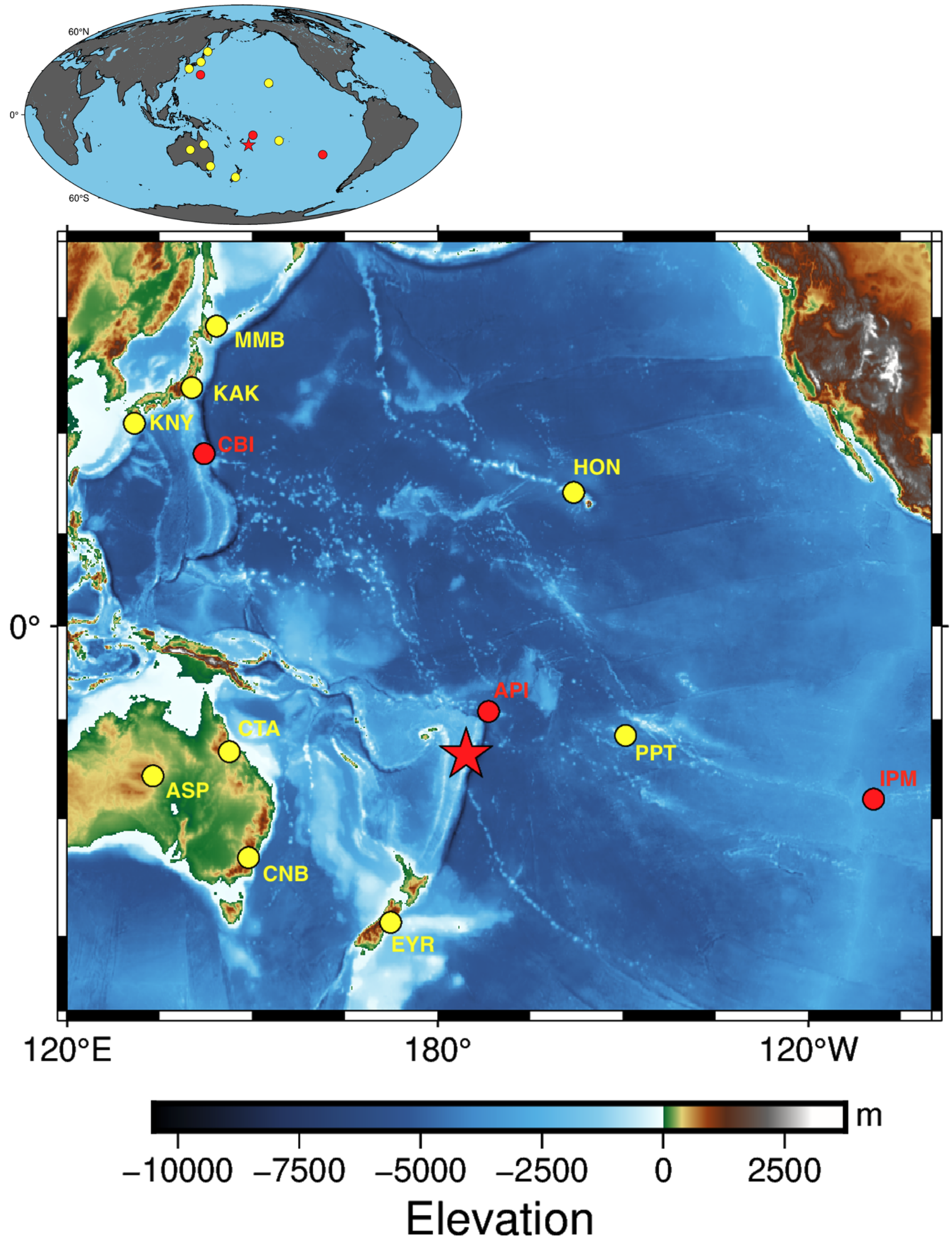

Figure 1. Map of the geomagnetic observatories (red circles for observatories with probable event signatures, yellow circles for regional observatories used in cross-wavelet analysis) used to study the magnetic signals induced by the Hunga Tonga–Hunga Ha'apai eruption. Location of the eruption is given by the red star.

turbations on the ocean surface and that the tsunami water wave's arrival is after that initial onset (Kubota et al., 2022). Regardless, the event water arrival time for high pass filtering with a maximum period (T_{max}) of 30 minutes are within 10 minutes to those estimated using $T_{max} = 120$ minutes. These arrival times are labeled on the figures.

For API, the magnetic signal appears to arrive before the water wave. However, because the water level station is on a further island from the geomagnetic observatory, the magnetic signals may in fact be concurrent with the water waves' arrival at the geomagnetic observatory.

2.3 Identifying local signals via cross-wavelet analysis

To examine the time-frequency characteristics of the signals, as well as isolate the signals that are local to a given observatory, we used the cross-wavelet analysis (C-WA) methodology developed in Schnepf et al. (2016). This method performs a wavelet analysis on the horizontal and vertical magnetic field components at both a local observatory and a remote observatory. The horizontal wavelet matrices are then crossed to produce a weighing matrix so that features common to both the local and remote observatory are then down-weighed in the local vertical wavelet matrix. This weighing matrix linearly depends on the crossed amplitudes– it is best suited for geomagnetically quiet conditions. When the common external signals significantly vary in amplitude, then the weight matrix is skewed towards diminishing the common large amplitude outlier events and there can be leakage of lower amplitude common signals. This may be why the C-WA results for the Japanese observatories of KAK, KNY, and MMB show so many similar signals (Supplementary Figures S21-S22).

The wavelet and cross-wavelet analysis was performed on both the time series resulting from the $T_{max} = 30$ minutes and $T_{max} = 120$ minutes high pass filtering. Figures 2 - 4 shows the down-weighed local vertical wavelet matrix at API, CBI, and IPM for both $T_{max} = 30$ minutes and $T_{max} = 120$ minutes. For all observatories, the cross-wavelet analysis was performed using ASP as the remote observatory. Results at other stations are presented in the Supplementary Information (Figures S21-S26).

3 Results and Discussion

The largest January 2022 eruption of Hunga Tonga–Hunga Ha'apai occurred at about 04:00 UTC on January 15th. This day was somewhat disturbed in terms of geomagnetic activity indices. Fortunately, most of the disturbed times were before the eruption or long after signals from the event would have reached Pacific observatories. According to the German Research Centre for Geosciences (GFZ), from 00-03 UTC, the planetary K (Kp) index was 5, from 03-09 and 12-18 it was a quiet index of 3, 09-12 it was an even quieter index of 2, from 18-21 it was 4 and from 21-24 it was 5 (shown in Supplementary Figure S1).

To remove regional magnetic signals from magnetospheric sources we used the cross-wavelet analysis (C-WA) method (Schnepf et al., 2016) with ASP as the reference station. This method can allow leakage of lower amplitude common signals if there are common large amplitude outlier events. We compare our results at several observatories to ensure that the signals we identify are local.

Shown in Figure 2, the event's water wave reached Samoa by 05:12 UTC (for the $T_{max} = 30$ minutes high-pass filtered, HPF, data). Magnetic signals with periods of 3-8 minutes and strengths of $\sim$1 nT arrived at API starting at 04:44 UTC and persisting until 05:38 UTC. These high frequency signals were not visible at any other geomagnetic observatory in the region– none of the other considered geomagnetic observatories had magnetic signals with periods under 5 minutes. Interestingly, the high frequency sig-

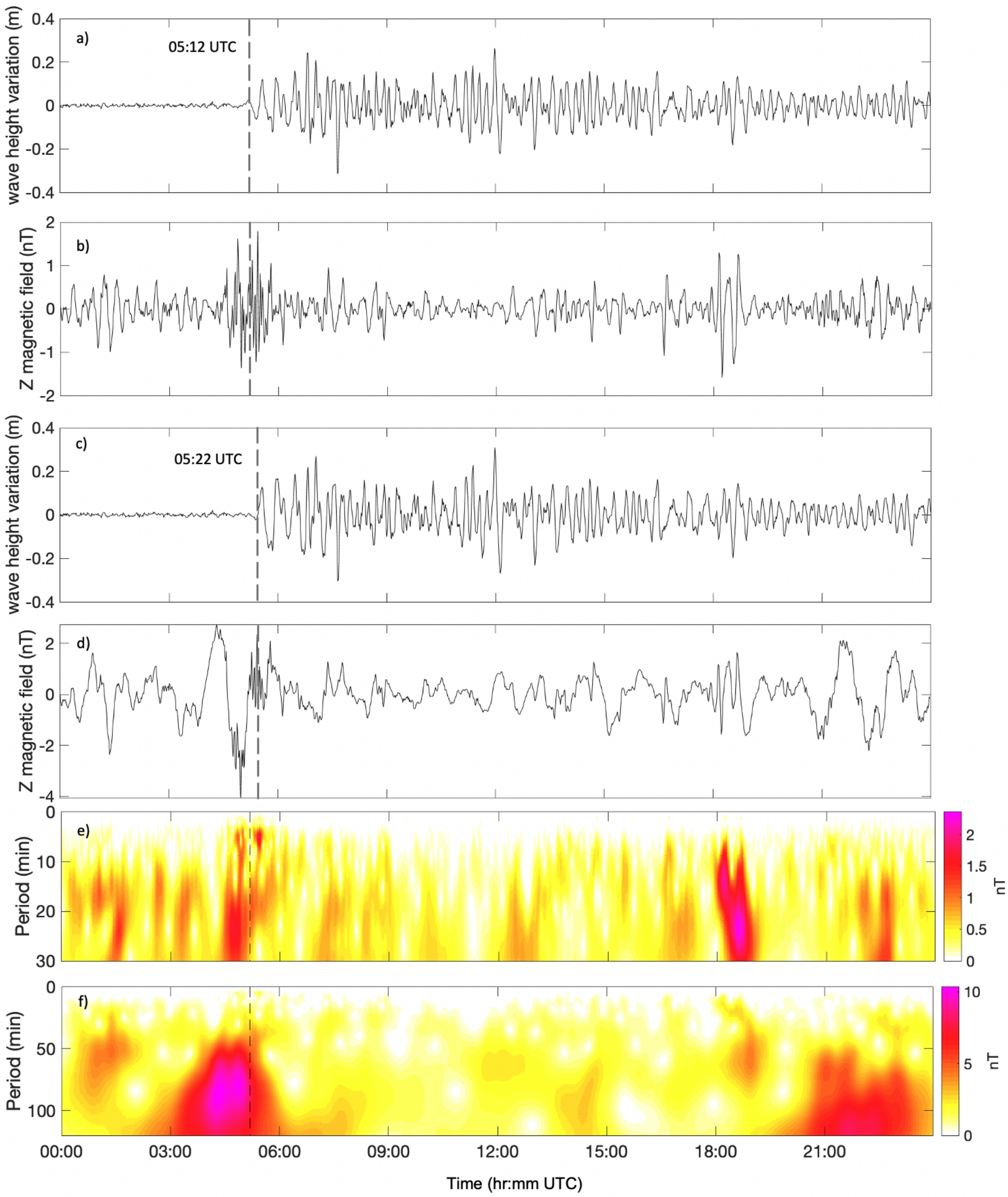

Figure 2. The water and magnetic field data for API after undergoing a high pass filter with a maximum period of 30 minutes (respectively, rows a and b) and 120 minutes (respectively, rows c and d). API's down-weighed Z wavelet matrix is shown in row e for a maximum period of 30 minutes and in row f for a maximum period of 120 minutes. For rows e and f the dashed line corresponds to the 05:12 UTC water wave arrival time.

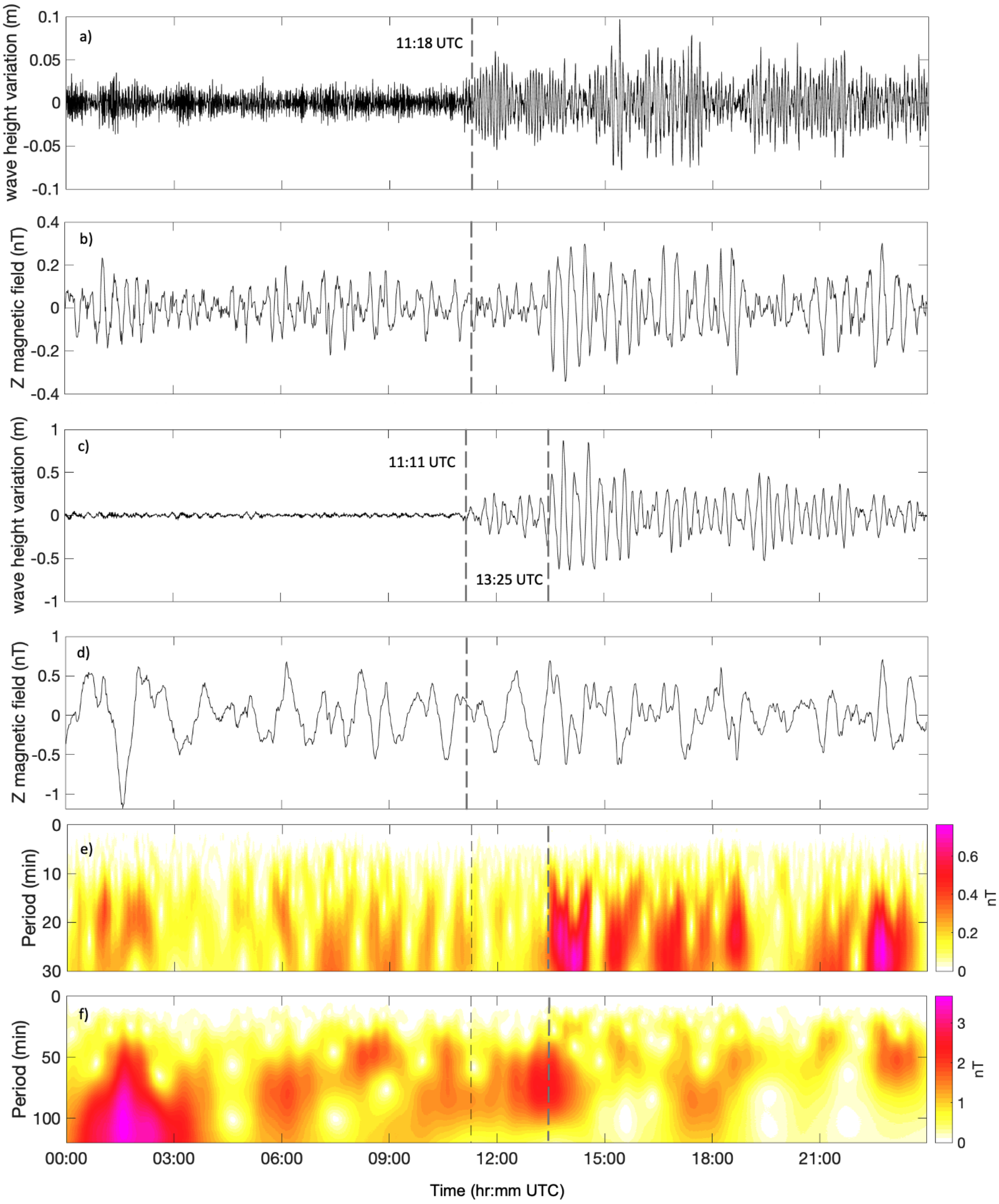

Figure 3. The water and magnetic field data for CBI after undergoing a high pass filter with a maximum period of 30 minutes (respectively, rows a and b) and 120 minutes (respectively, rows c and d). CBI's down-weighed Z wavelet matrix is shown in row e for a maximum period of 30 minutes and in row f for a maximum period of 120 minutes. For rows e and f the first dashed line corresponds to the 11:11 UTC water wave arrival time and the second corresponds to the 13:25 UTC larger amplitude water wave arrival time seen in row c.

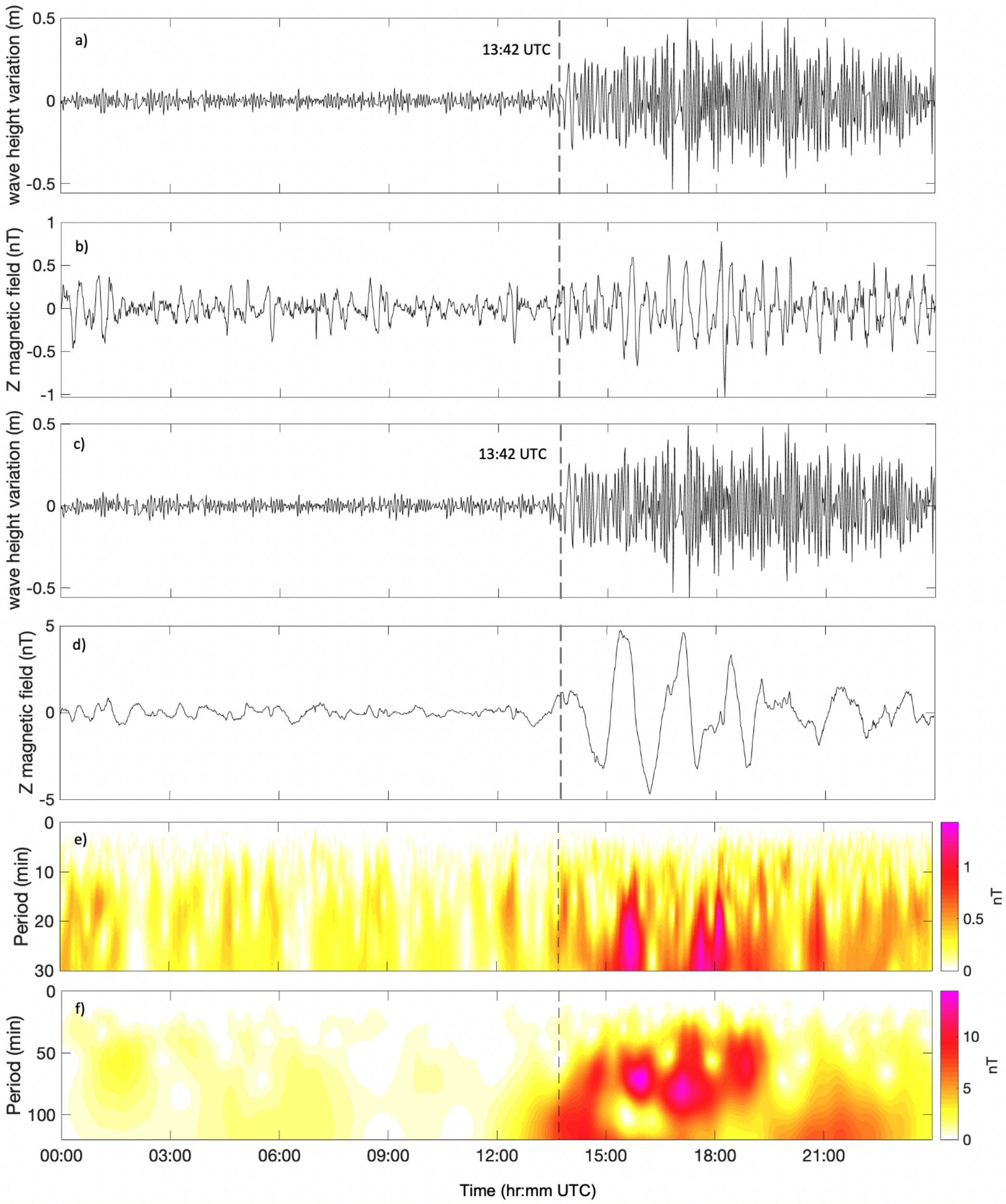

Figure 4. The water and magnetic field data for IPM after undergoing a high pass filter with a maximum period of 30 minutes (respectively, rows a and b) and 120 minutes (respectively, rows c and d). IPM's down-weighed Z wavelet matrix is shown in row e for a maximum period of 30 minutes and in row f for a maximum period of 120 minutes. For rows e and f the dashed line corresponds to the 13:42 UTC water wave arrival time.

nals were in both API's Z and H magnetic field components (Supplementary Figure S13). Oceanic magnetic fields should only be detectable in the vertical component of coastal observatories. This suggests the signals are external in nature. Additionally, the period range of API's magnetic signature also fits with that of traveling ionospheric disturbances (TIDs) and acoustic resonance between the ground and ionosphere (Iyemori et al., 2005). This signal is most likely due to ionospheric sources and this station's close proximity to the eruption could explain why it was the only observatory with signals < 5 minutes period. To definitively separate the sources at play here, future studies should use a combination of data sources, methods that separate external and internal magnetic fields, and perhaps numerical simulations of the expected tsunami or ionospheric signal.

At CTA, CNB, and EYR, C-WA results reveal common signals between 06-09 UTC for longer periods ($\sim$15-120 minutes; shown in Supplementary Figures S23-S24). In the C-WA results for $T_{max} = 30$ minutes, API, and CNB both have recurring signals within a period range of 15-30 minutes spanning from about 06-18 UTC. All of the observatories considered in this study, except for CTA, have recurring magnetic signals occurring after 18:00 UTC. Because 18:00 is when the Kp index became disturbed, a more rigorous study focused on external fields/sources is needed to convincingly establish whether these recurring signals are due to the eruption's atmospheric/ionospheric effects or to space weather.

Long period signals (50-120 min) at API are strongest between the time of eruption and the water wave's arrival, however, this longer period signal commences before the largest eruption, so it is unclear if this is volcano related or due to space weather. Interestingly, CTA, CNB, and EYR all have longer period signals occurring between 06-09 UTC, and CNB and EYR have a recurring signal within the $\sim$50-110 minutes period range. Again, further studies focused on external fields/sources would be useful for evaluating these signals.

At CBI, magnetic signals were coincident with the arrival of 1m-varying water waves (13:25 UTC, evident in Figure 3b-c,e-f). The dominant period range of the $T_{max} = 30$ minutes HPF signature is $\sim$13-19 minutes with corresponding amplitudes of 0.4-0.7 nT. For the lower frequency C-WA results (Figure 3f), the signal is smeared across the 13:25 UTC arrival time and the corresponding period range is 49-93 minutes with amplitudes of 1.8-2.4 nT. It is not surprising that the period range extends to $\sim$1.5 hours, after all, in Figure 3e there are magnetic signals recurring with roughly that periodicity.

The other Japanese observatories (KAK, KNY, and MMB) have many recurring magnetic signals throughout January 15th (Supplementary Figures S21-S22). Considering that KAK, KNY, and MMB are all fairly inland, and how similar the signals are across the three observatories, these recurring signals must be external in origin. Determining whether these external signals are due to post-eruption ionospheric waves or a geomagnetic storm is beyond the scope of this study.

At IPM, magnetic signals were coincident with the 13:42 UTC water wave arrival (Figure 4). The high-pass filtered Z magnetic field data shows this most obviously when $T_{max} = 120$ minutes, however, signals are evident for both $T_{max} = 30$ and $T_{max} = 120$ minutes in the C-WA results (Figure 4e-f). Along with the initial magnetic signal, IPM has magnetic signals of 5-100+ minute periodicity coincident with the water wave and returning roughly every hour. The amplitude of the signal is greater for larger periods: it is 0.7 nT near the water wave arrival for a period of 17 minutes and 5-14 nT near the peaks that have periods of 60-90 minutes.

For both period ranges, PPT and HON do not have any magnetic signals obviously concurrent with the water wave arrival (Supplementary Figures S25-S26) . This may be due to their location: while they are on islands, both of these observatories have anthropogenic electromagnetic sources resting between them and the sea. Thus, instead of signals comparable to IPM, CBI, or API, there are recurrent signals throughout the day at HON and starting at 12:00 UTC for PPT. Some of the recurring signals appear similar to those repeating at the Japanese stations so they likely are external signals, perhaps related to the eruption or related to the Kp index increasing after 18 UTC. Either way, for $T_{max} = 120$ minutes, PPT and HON have recurring signals starting at 16:10 UTC and 16:25, respectively. This suggests that the signals at IPM occurring between the 13:42 UTC water wave arrival and ∼16 UTC are truly local magnetic signatures arising from the eruption.

It is unclear whether the signals at CBI and IPM are due to the eruption's tsunami water wave, deformation of the sea surface from atmospheric acoustic waves, or ionospheric waves. Indeed, the magnetic signatures at CBI, IPM, and API likely stem from a combination of these sources.

4 Conclusions and Outlook

January 15, 2022 started and ended with disturbed geomagnetic conditions but conditions were relatively quiet around the time of the Hunga Tonga–Hunga Haʻapai eruption and stayed quiet through to when oceanic and atmospheric waves from the explosion reached the various Pacific geomagnetic observatories.

The local magnetic signature at API had periods of 3-8 minutes and strengths of ∼1 nT arrived starting at 04:44 UTC and persisting until 05:38 UTC. API's magnetic signature is most likely due to ionospheric sources.

For Chichijima Island (CBI, Japan) and Easter Island (IPM, Chile), the local magnetic signals were concurrent with the eruption's water wave arrivals. At CBI, the magnetic signatures had period bands of 13-19 minutes (with corresponding amplitudes of 0.4-0.7 nT) and 49-93 minutes (with corresponding amplitudes of 1.8-2.4 nT). Meanwhile, at IPM, we identified magnetic signatures of 5-100+ minute periodicity and 5-14 nT amplitude. It is unclear whether the signals at CBI and IPM are due to the eruption's tsunami water wave, deformation of the sea surface from atmospheric acoustic waves, ionospheric waves, or combinations of all these eruption-induced sources.

The Honolulu (HON) and Tahiti (PPT) observatories lacked clear magnetic signals concurrent with their island's water wave arrival time. Instead, similar to the other more inland observatories used in this study, recurrent magnetic signals were seen for the bulk of January 15th. These signals must be external in original, however, it is ambiguous if they are related to the Hunga Tonga–Hunga Haʻapai eruption or to Earth's space weather conditions.

Future studies should pursue methods that separate internal and external magnetic field sources at each of the near-sea observatories. Additionally, incorporating atmospheric pressure data or ionospheric total electron content data could help distinguish the different sources creating the identified magnetic signatures. Numerical studies may also shed light in separating the magnetic signal from the tsunami water wave and the ionospheric disturbances. With such future work, we believe that the magnetic signatures from submarine volcanic eruptions can be rendered sensible.

5 Data Availability Statement

With the exception of the Chichijima and Honolulu stations, magnetic field observatory data is available available through INTERMAGNET (`www.intermagnet.org`). Data from CBI at Chichijima station was obtained from the Japanese Meteorological Agency and may be accessed by contacting Kakioka Magnetic Observatory, JMA (`http://www.kakioka-jma.go.jp/en/`). Data from HON at Honolulu was obtained from the Kyoto World Data Centre for Geomagnetism (`http://wdc.kugi.kyoto-u.ac.jp/`) and the station is supported/maintained by the U.S. Geological Survey.

Water level data for Honolulu, USA was obtained from the National Oceanic and Atmospheric Administration's Tides and Currents website, developed and supported by the Center for Operational Oceanographic Products and Services (CO-OPS): `https://tidesandcurrents.noaa.gov/products.html`. Water level data for Chichijima Island was obtained from the Japanese Meteorological Agency. For Western Samoa, Easter Island, and Tahiti, water level data was accessed from the w's Flanders Marine Institute sea level station monitoring facility (VLIZ, 2022) and is accessible at: `http://www.ioc-sealevelmonitoring.org`.

All scripts used for data processing, as well as prepared Matlab data files for both the geomagnetic and water level data, may be accessed at `https://github.com/NeeshaRS/geomag_tsunamis/tree/main/tsunami_library` and `https://github.com/NeeshaRS/geomag_tsunamis/tree/main/2022_Tonga`.

Acknowledgments

The results presented in this paper rely on data collected at magnetic observatories. We thank the national institutes that support them: the Japanese Meteorological Agency, the U.S. Geologic Survey, Geoscience Australia, New Zealand's Institute of Geological and Nuclear Sciences, Bureau Central de Magnétism Terrestre. We also thank INTERMAGNET for promoting high standards of magnetic observatory practice (www.intermagnet.org). We utilized data collected at tide gauge facilities and sea-level monitoring sites. We thank the National Oceanic and Atmospheric Administration, the Japanese Meteorological Agency, and the Flanders Marine Institute for the water level data used in this study. N.R.S. would also like to thank K. Tiampo and D. Brain for useful discussions. This work was supported by a Grant-in-Aid for Scientific Research (19K03993) from the Japan Society for the Promotion of Science. The authors declare no conflicts of interest.

References

Astafyeva, E. (2019). Ionospheric detection of natural hazards. *Reviews of Geophysics*, *57*(4), 1265-1288. doi: 10.1029/2019RG000668

Dautermann, T., Calais, E., Lognonné, P., & Mattioli, G. S. (2009, 12). Lithosphere—atmosphere—ionosphere coupling after the 2003 explosive eruption of the Soufriere Hills Volcano, Montserrat. *Geophysical Journal International*, *179*(3), 1537-1546. doi: 10.1111/j.1365-246X.2009.04390.x

Dautermann, T., Calais, E., & Mattioli, G. S. (2009). Global Positioning System detection and energy estimation of the ionospheric wave caused by the 13 july 2003 explosion of the Soufrière Hills Volcano, Montserrat. *Journal of Geophysical Research: Solid Earth*, *114*(B2). doi: 10.1029/2008JB005722

Faraday, M. (1832). The bakerian lecture: Experimental researches in electricity. second series. terrestrial magneto-electric induction. *Philosophical Transactions of the Royal Society of London*, *122*, 163-194.

Heki, K. (2006). Explosion energy of the 2004 eruption of the Asama Volcano, central Japan, inferred from ionospheric disturbances. *Geophysical Research Letters*, *33*(14). doi: https://doi.org/10.1029/2006GL026249

Ichihara, H., Hamano, Y., Baba, K., & Kasaya, T. (2013). Tsunami source of the 2011 tohoku earthquake detected by an ocean-bottom magnetometer. *Earth and Planetary Science Letters*, *382*, 117–124. doi: 10.1016/j.epsl.2013.09.015

Iyemori, T., Nose, M., Han, D., Gao, Y., Hashizume, M., Choosakul, N., ... Yang, F. (2005). Geomagnetic pulsations caused by the Sumatra earthquake on December 26, 2004. *Geophysical Research Letters*, *32*(20). doi: https://doi.org/10.1029/2005GL024083

Klausner, V., Kherani, E. A., & Muella, M. T. A. H. (2016). Near- and far-field tsunamigenic effects on the z component of the geomagnetic field during the japanese event, 2011. *Journal of Geophysical Research: Space Physics*, *121*(2), 1772–1779. doi: 10.1002/2015JA022173

Kubota, T., Saito, T., & Nishida, K. (2022). Global fast-traveling tsunamis by atmospheric pressure waves on the 2022 tonga eruption. *Earth arXiv preprint*. doi: 10.31223/X5KP8M

Lin, Z., Toh, H., & Minami, T. (2021). Direct comparison of the tsunami-generated magnetic field with sea level change for the 2009 samoa and 2010 chile tsunamis. *Journal of Geophysical Research: Solid Earth*, *126*(11). doi: 10.1029/2021JB022760

Liu, X., Zhang, Q., Shah, M., & Hong, Z. (2017). Atmospheric-ionospheric disturbances following the April 2015 Calbuco volcano from GPS and OMI observations. *Advances in Space Research*, *60*(12), 2836-2846. doi: 10.1016/j.asr.2017.07.007

Manoj, C., Maus, S., & Chulliat, A. (2011). Observation of magnetic fields generated by tsunamis. *Eos, Transactions American Geophysical Union*, *92*(2), 13–14. doi: 10.1029/2011EO020002

Minami, T., Schnepf, N. R., & Toh, H. (2021). Tsunami-generated magnetic fields have primary and secondary arrivals like seismic waves. *Scientific Reports*, *11*(1), 2287. doi: 10.1038/s41598-021-81820-5

Minami, T., Toh, H., Ichihara, H., & Kawashima, I. (2017). Three-dimensional time domain simulation of tsunami-generated electromagnetic fields: Application to the 2011 tohoku earthquake tsunami: Simulation of tsunami magnetic signals. *Journal of Geophysical Research: Solid Earth*, *122*(12), 9559–9579. doi: 10.1002/2017JB014839

Nakashima, Y., Heki, K., Takeo, A., Cahyadi, M. N., Aditiya, A., & Yoshizawa, K. (2016). Atmospheric resonant oscillations by the 2014 eruption of the Kelud volcano, Indonesia, observed with the ionospheric total electron contents and seismic signals. *Earth and Planetary Science Letters*, *434*, 112-116. doi: https://doi.org/10.1016/j.epsl.2015.11.029

Schnepf, N. R., Manoj, C., An, C., Sugioka, H., & Toh, H. (2016). Time-frequency characteristics of tsunami magnetic signals from four Pacific Ocean events. In *Global tsunami science: Past and future, volume i* (pp. 3935–3953). Springer. doi: 10.1007/s00024-016-1345-5

Sennert, S. K. (Ed.). (2022). *Global Volcanism Program, 2022. Report on Hunga Tonga-Hunga Ha'apai (Tonga).* Smithsonian Institution and US Geological Survey.

Shults, K., Astafyeva, E., & Adourian, S. (2016). Ionospheric detection and localization of volcano eruptions on the example of the april 2015 calbuco events. *Journal of Geophysical Research: Space Physics*, *121*(10), 10,303-10,315. doi: 10.1002/2016JA023382

Sugioka, H., Hamano, Y., Baba, K., Kasaya, T., Tada, N., & Suetsugu, D. (2014). Tsunami: Ocean dynamo generator. *Scientific Reports*, *4*, 2045-2322. doi: 10.1038/srep03596

Tatehata, H., Ichihara, H., & Hamano, Y. (2015). Tsunami-induced magnetic fields detected at chichijima island before the arrival of the 2011 tohoku earthquake tsunami. *Earth, Planets and Space*, *67*(1), 185. doi: 10.1186/s40623-015-0347-3

Tiampo, K. (n.d.). personal communication.

Toh, H., Satake, K., Hamano, Y., Fujii, Y., & Goto, T. (2011). Tsunami signals from the 2006 and 2007 kuril earthquakes detected at a seafloor geomagnetic observatory. *Journal of Geophysical Research*, *116*(B2), B02104. doi: 10.1029/2010JB007873

Utada, H., Shimizu, H., Ogawa, T., Maeda, T., Furumura, T., Yamamoto, T., ...

Nagamachi, S. (2011). Geomagnetic field changes in response to the 2011 off the pacific coast of tohoku earthquake and tsunami. *Earth and Planetary Science Letters*, *311*(1), 11-27. doi: https://doi.org/10.1016/j.epsl.2011.09.036

VLIZ, F. M. I. (Ed.). (2022). *Sea level station monitoring facility.* Intergovernmental Oceanographic Commission (IOC). Retrieved from `http://www.ioc-sealevelmonitoring.org` doi: 10.14284/482

Geophysical Research Letters

Supporting Information for

Magnetic Signatures of the January 15 2022 Hunga Tonga–Hunga Ha`apai Volcanic Eruption

N. R. Schnepf[1], T. Minami[2], H. Toh[3], and M. C. Nair[4,5]

1- University of Colorado Boulder, Laboratory for Atmospheric and Space Physics, Boulder, 80305, USA

2- Kobe University, Department of Planetology, Kobe, 657-8501, Japan

3- Kyoto University, Data Analysis Centre for

Geomagnetism and Space Magnetism, Kyoto, 606-8502, Japan

4- University of Colorado Boulder, Cooperative Institute for Research in Environmental Sciences, Boulder, 80305, USA

5- National Oceanic and Atmospheric Administration, National Centers for Environmental Information, Boulder, 80305, USA

Contents of this file

Introduction

The figures here serve to complement those in the main paper. We provide more information on the locations of the Western Samoa, Honolulu, Easter Island, and Papeete observatories; raw data from each observatory; and the spectrograms resulting from the cross-wavelet analysis (for both a maximum period of 30 minutes and 120 minutes) of each observatory with the Alice Springs observatory.

Geomagnetic conditions

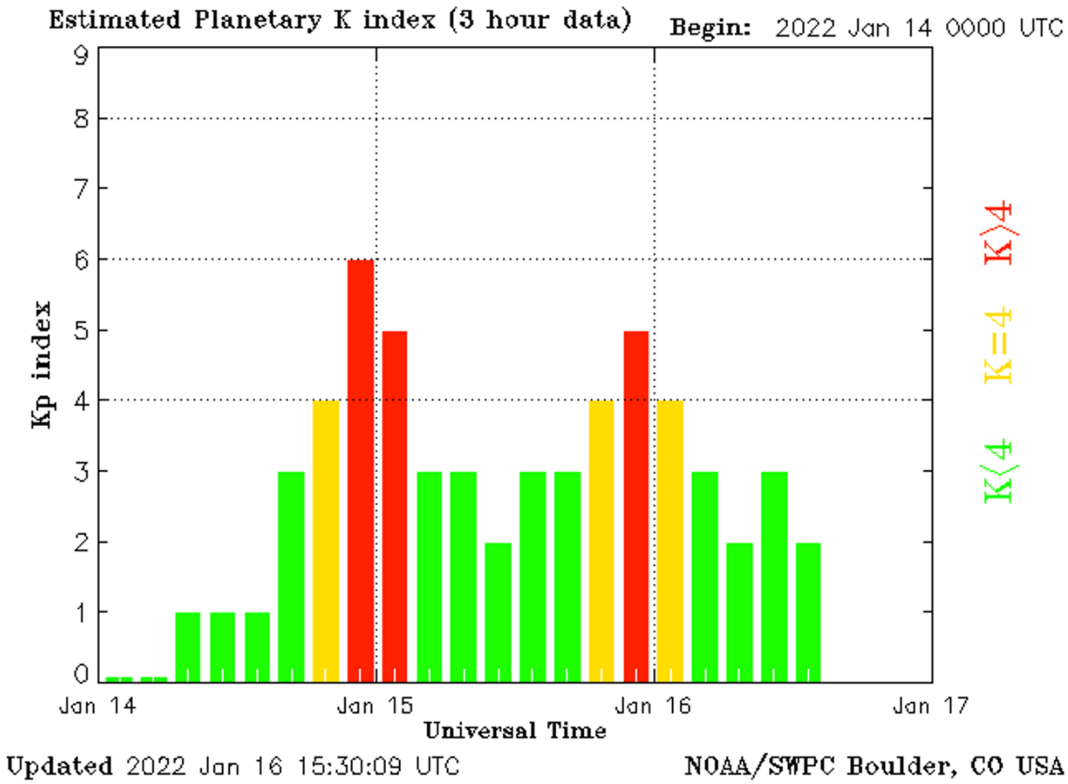

Figure S1. The Kp index on January 14-16, 2022 **.**

Detailed view of the observatory locations

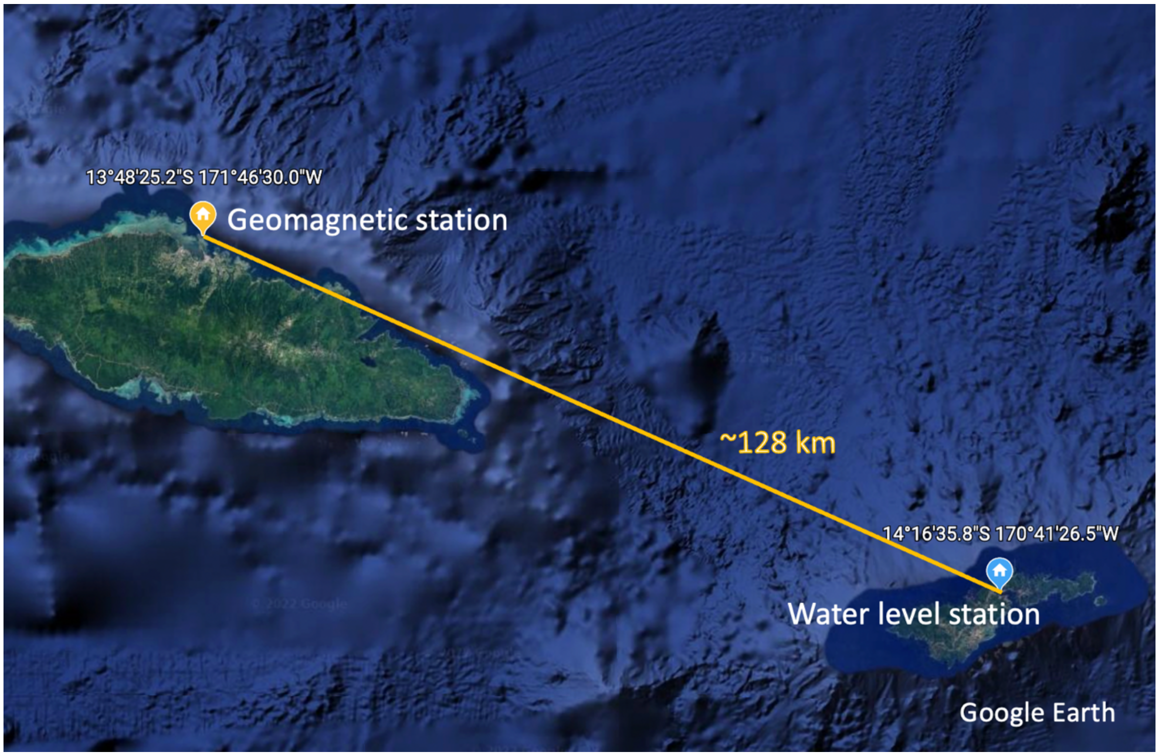

Figure S2. Location of the Western Samoa geomagnetic observatory relative to the water level station.

Figure S3. Location of the Honolulu, USA geomagnetic observatory relative to the coast.

Figure S4. Location of the Easter Island, Chile geomagnetic observatory relative to the coast.

Figure S5. Location of the Papeete, Tahiti, French Polynesia geomagnetic observatory relative to the coast.

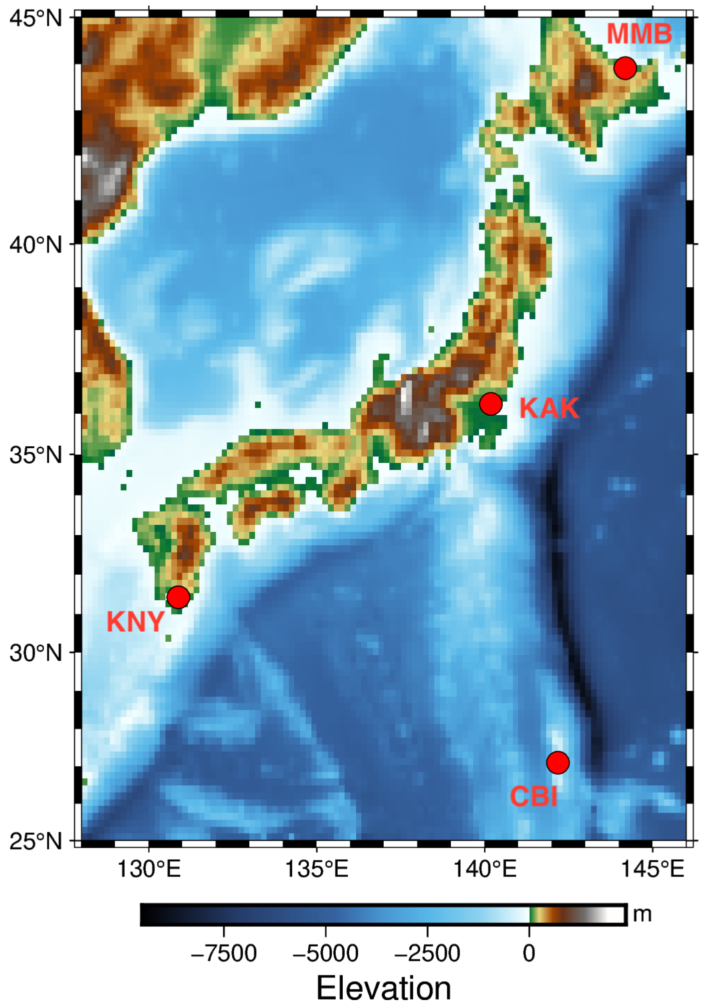

Figure S6. Map of the Japanese observatories.

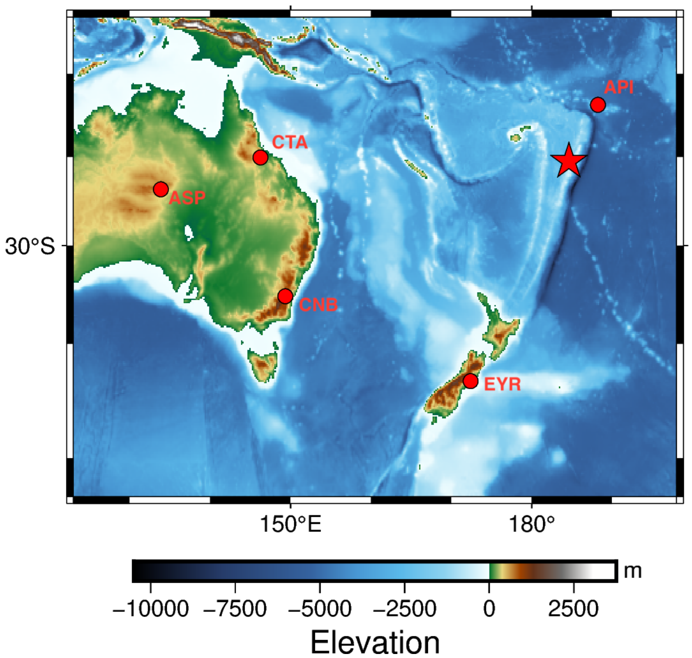

Figure S7. Map of the Oceania observatories.

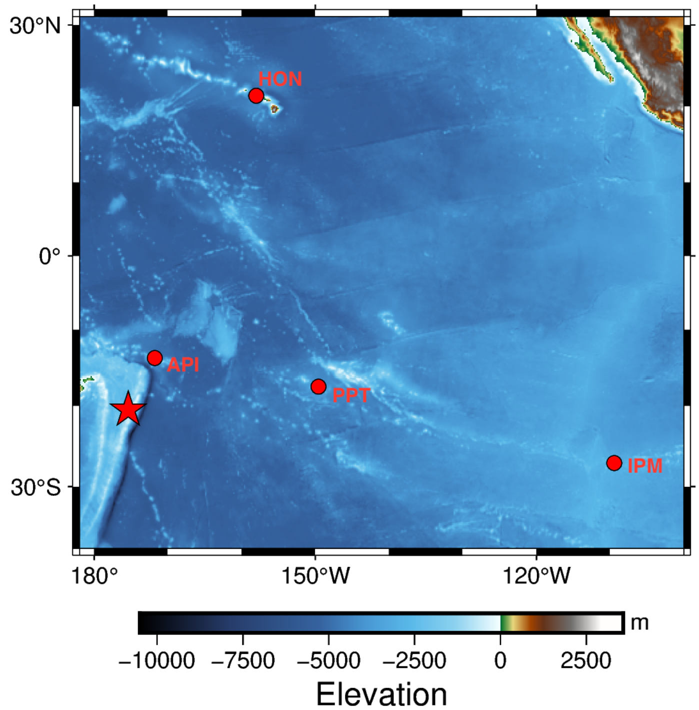

Figure S8. Map of the mid-Pacific observatories.

Raw data at Japanese observatories

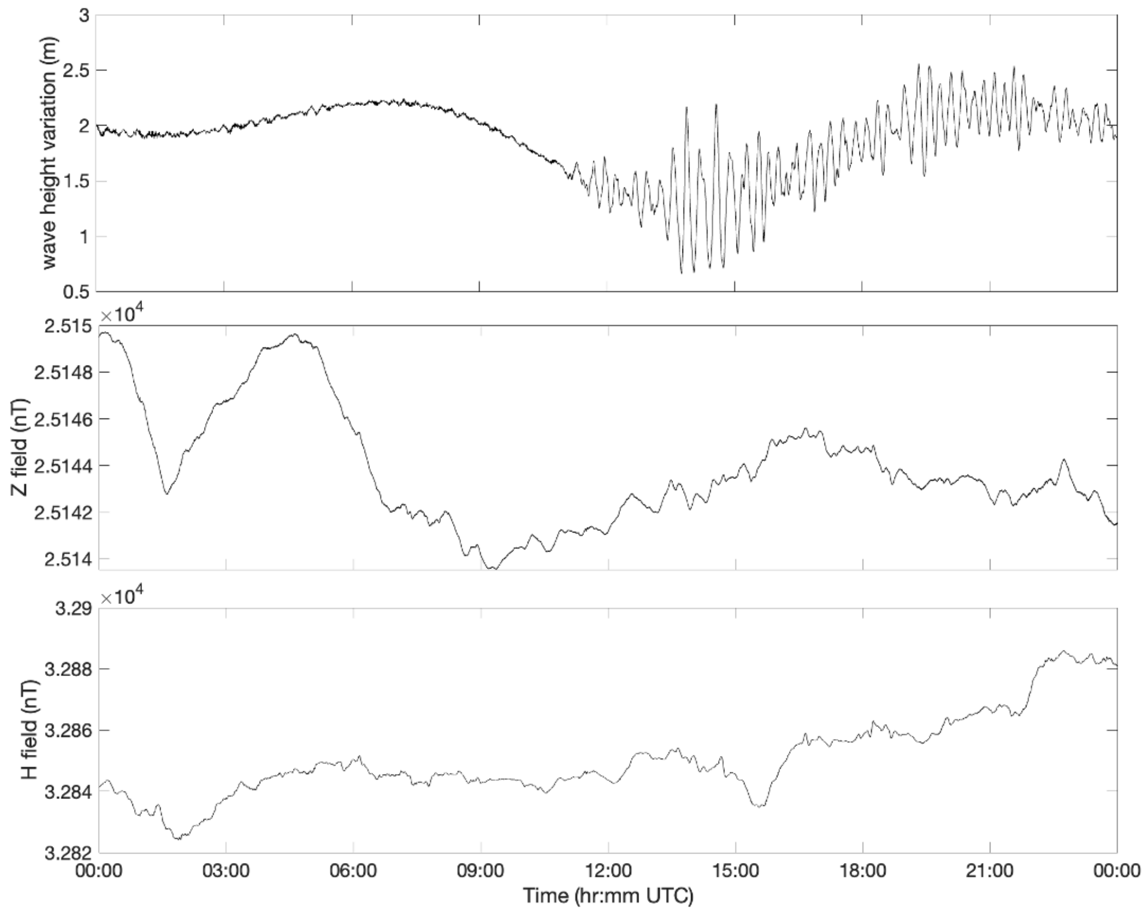

Figure S9. Raw water level variation and magnetic field data at Chichijimi Island (CBI).

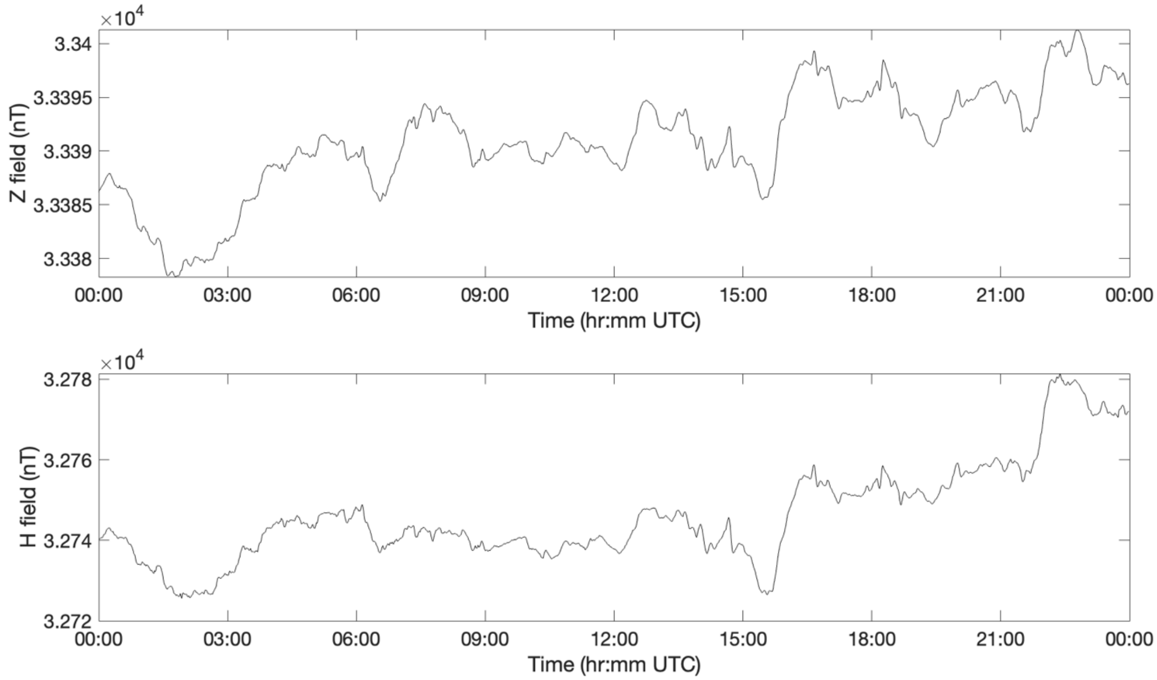

Figure S10. Raw magnetic field data at Kanoya (KNY).

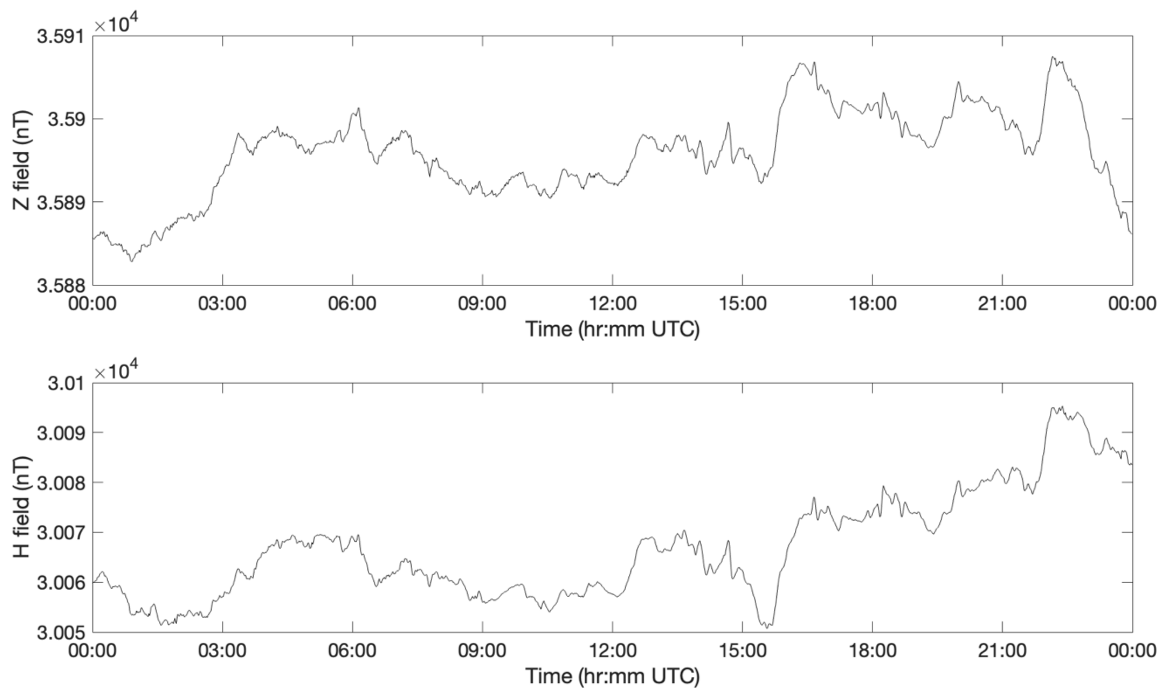

Figure S11. Raw magnetic field data at Kakioka (KAK).

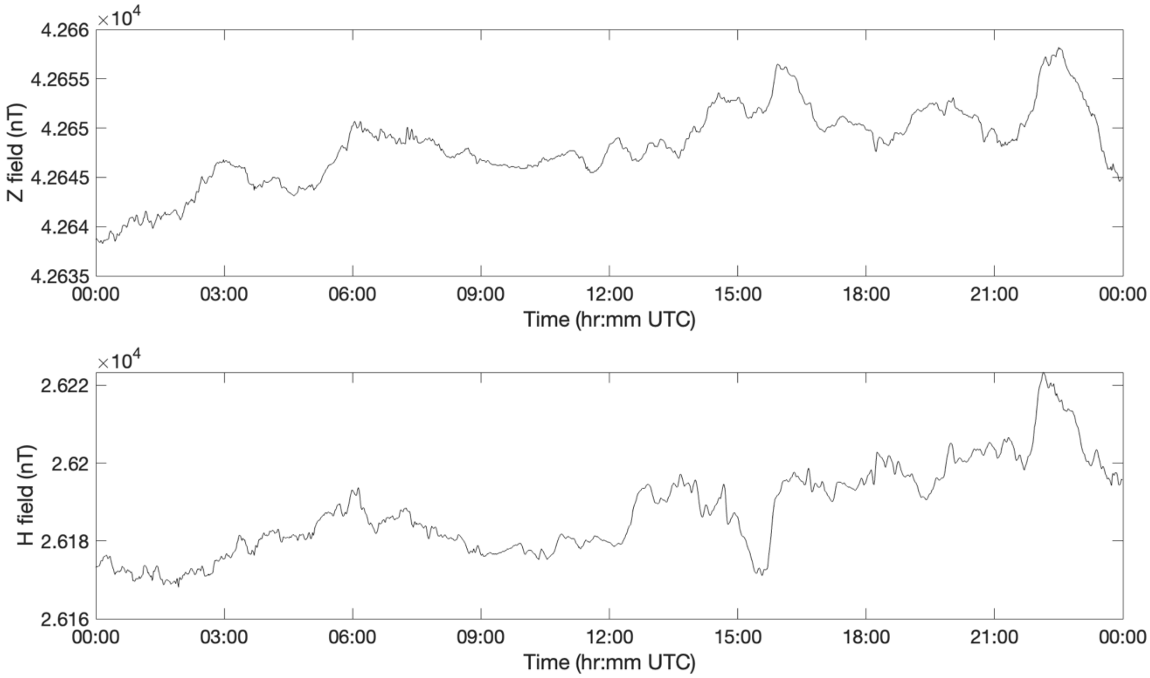

Figure S12. Raw magnetic field data at Memambetsu (MMB).

Raw data at Oceania observatories

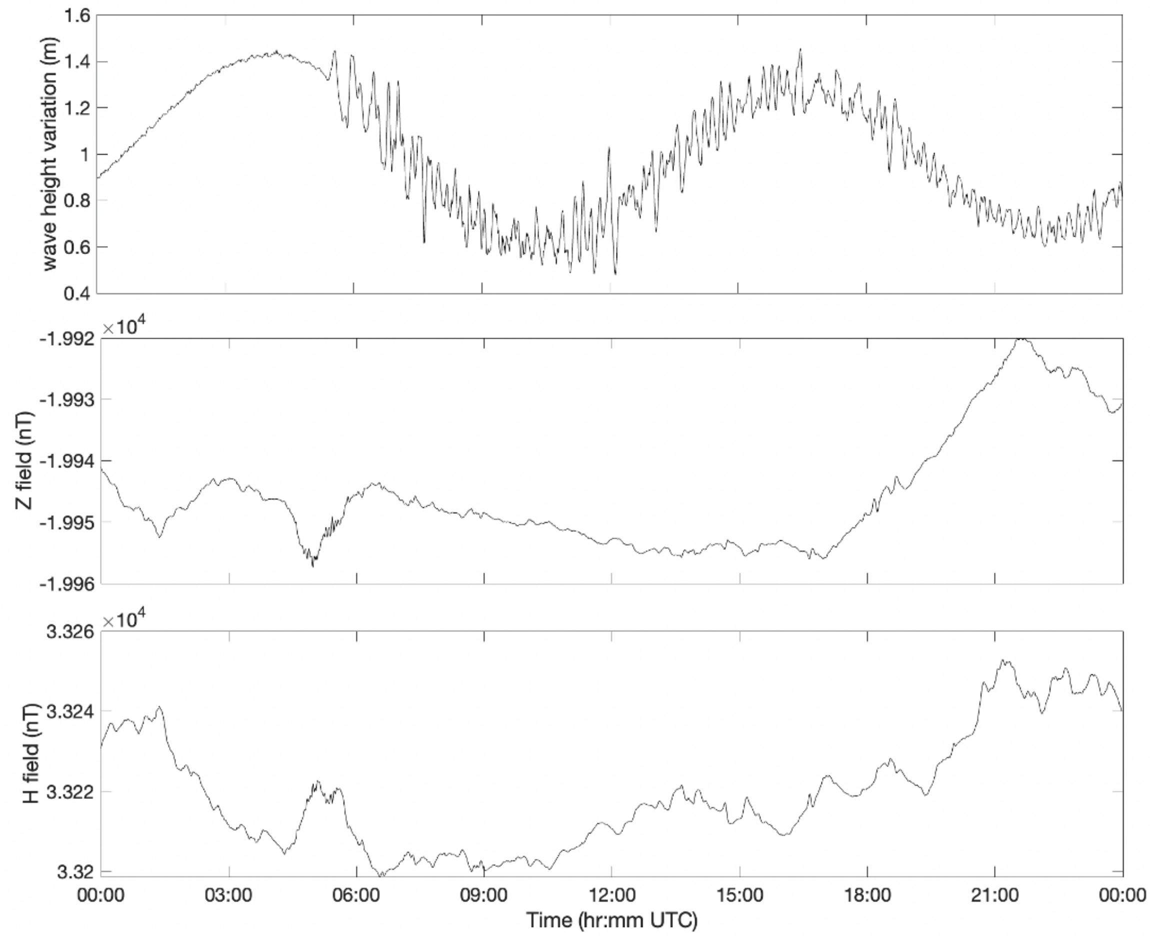

Figure S13. Raw water level variation and magnetic field data at Western Samoa (API).

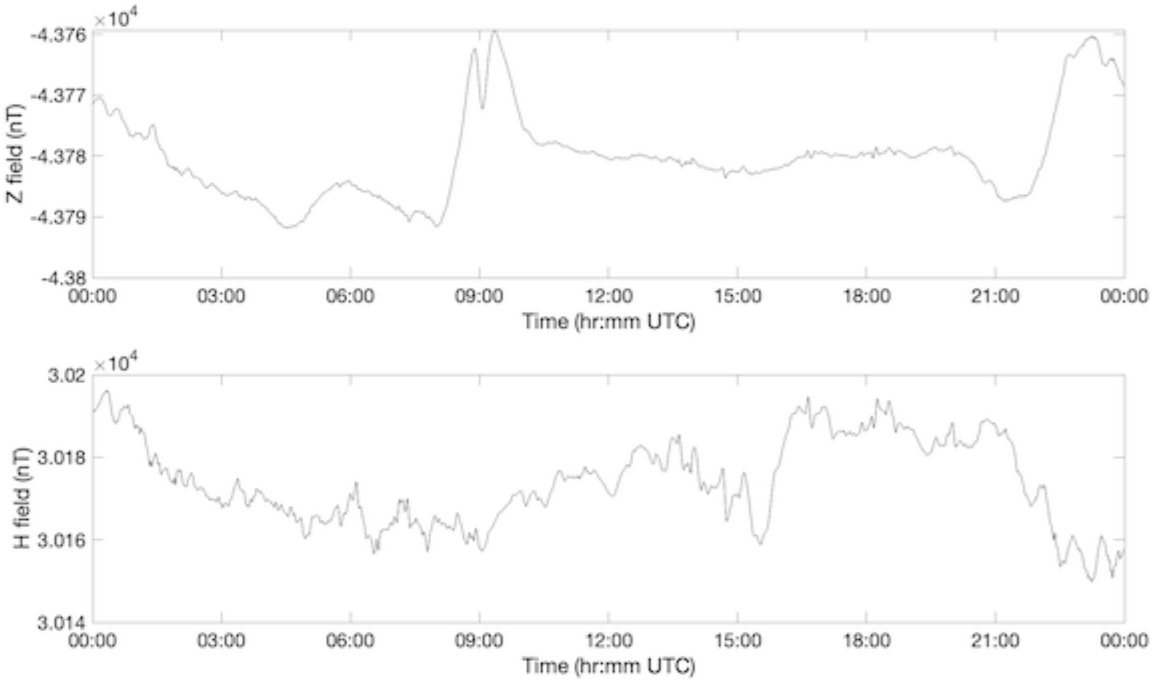

Figure S14. Raw magnetic field data at Alice Springs, Australia (ASP).

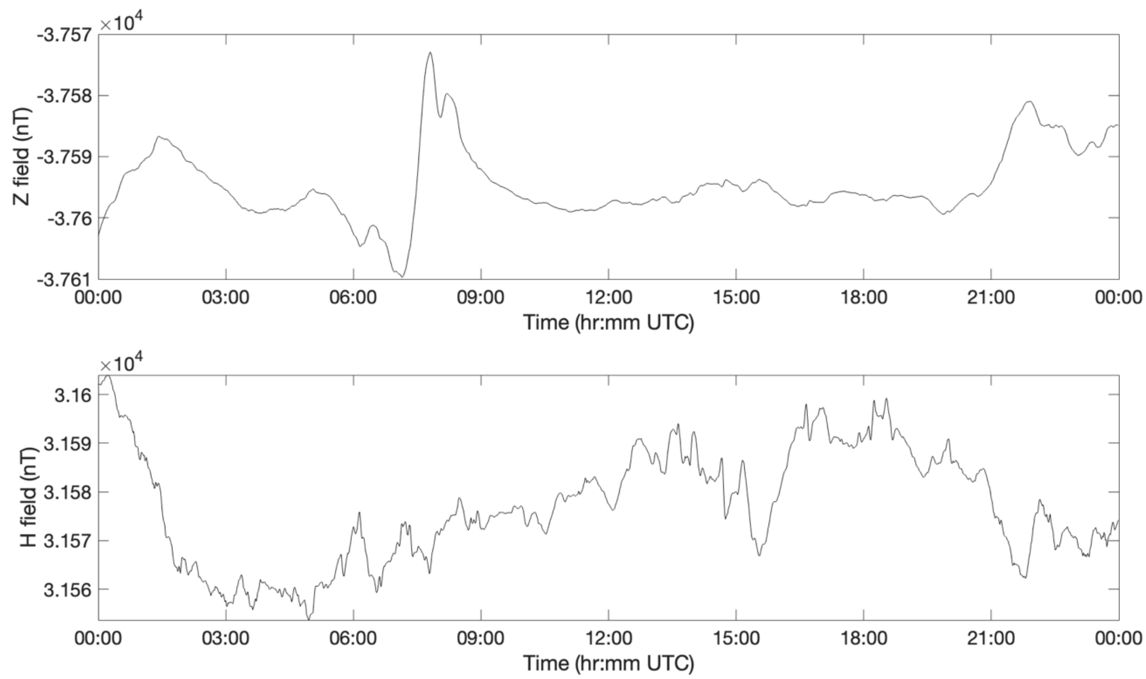

Figure S15. Raw magnetic field data at Charter Towers, Australia (CTA).

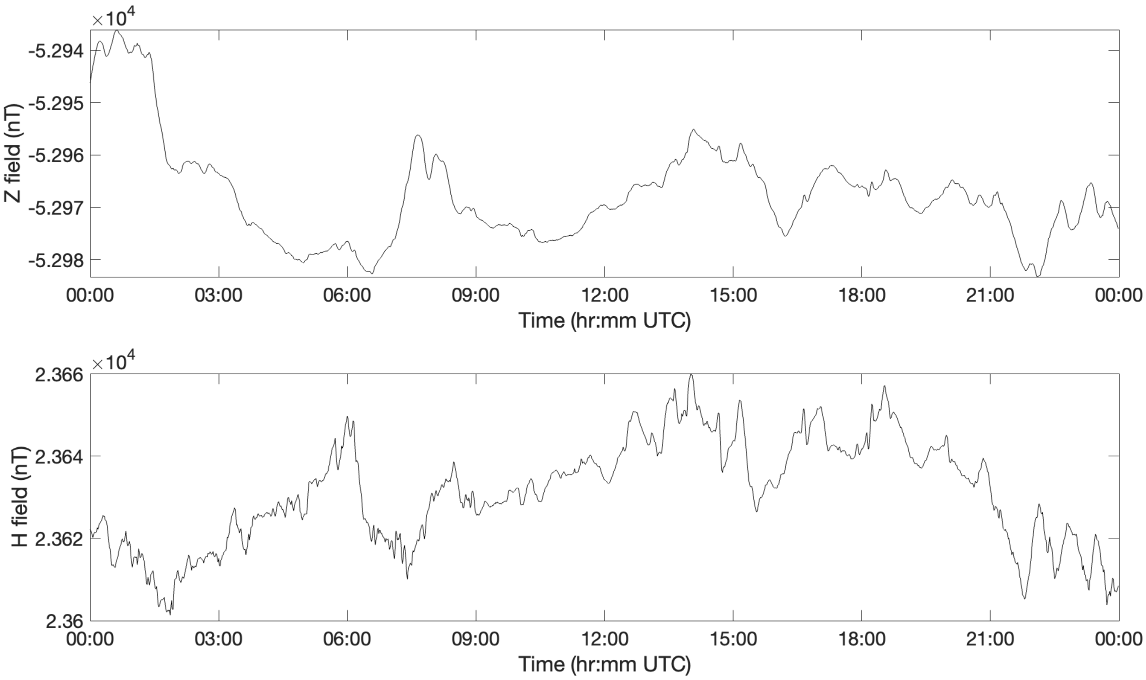

Figure S16. Raw magnetic field data at Canberra, Australia (CNB).

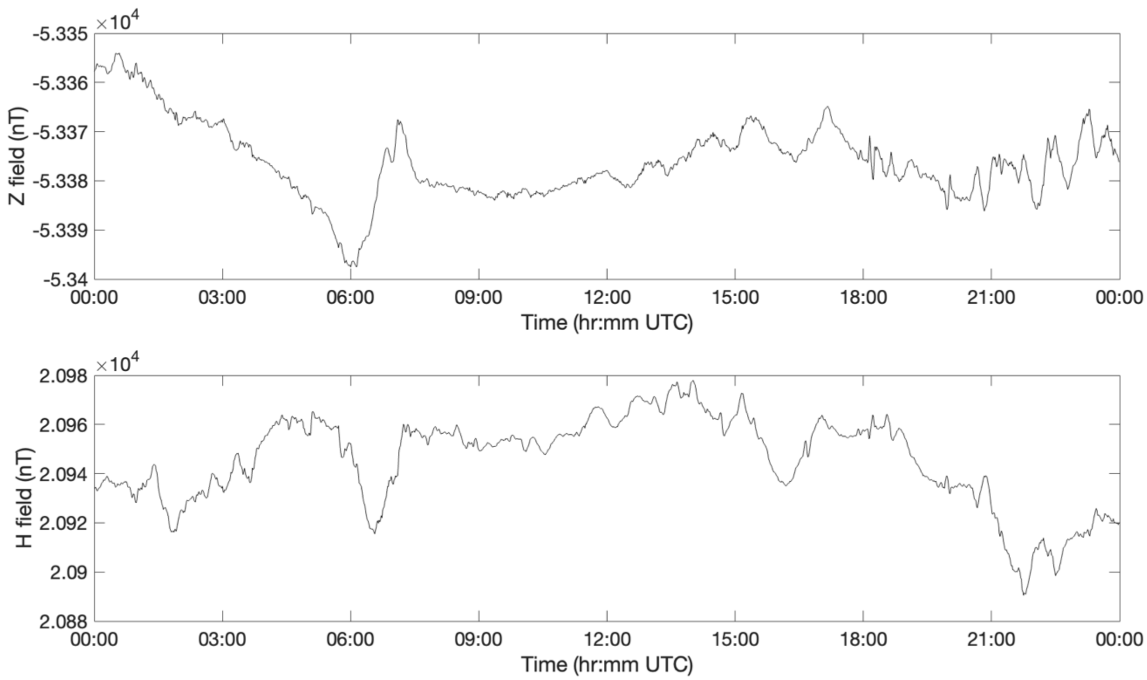

Figure S17. Raw magnetic field data at Eyrewell, New Zealand (EYR).

Raw data at mid-Pacific observatories

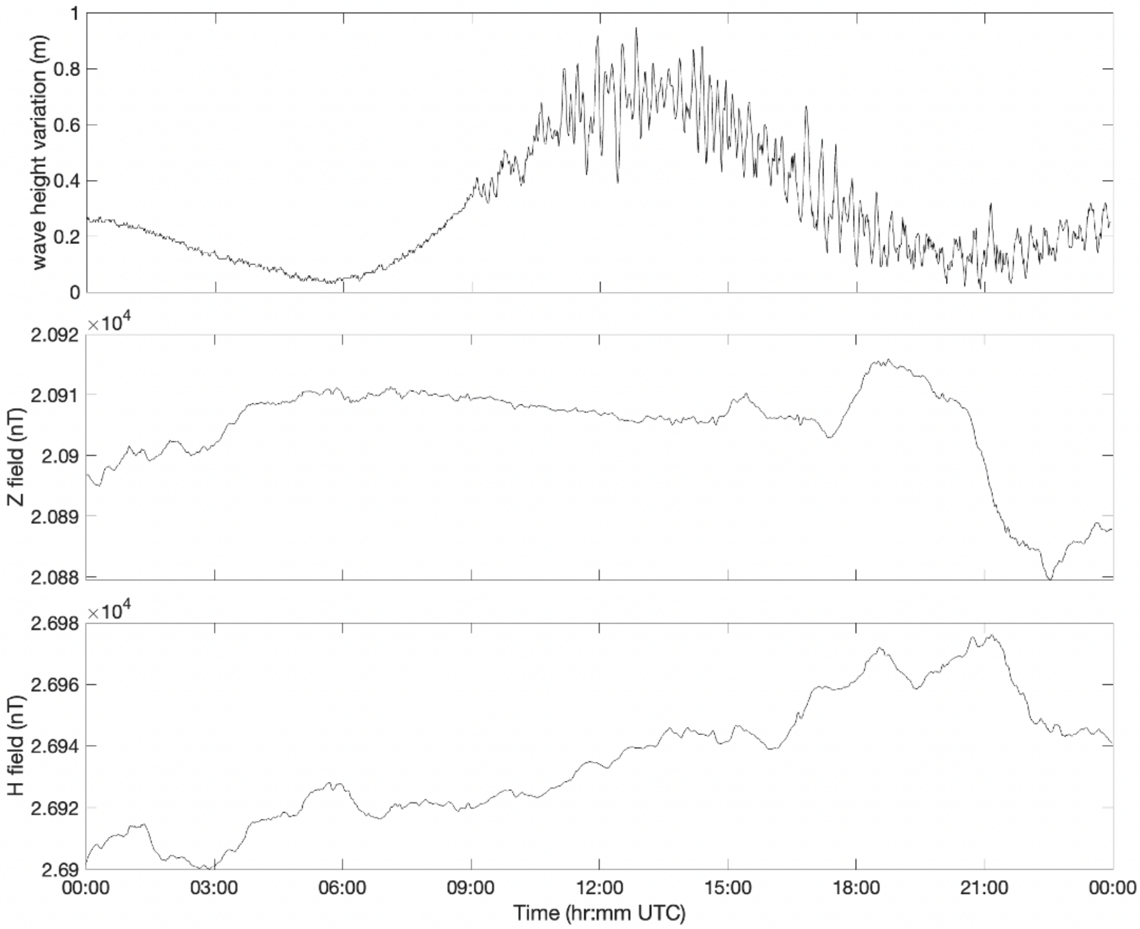

Figure S18. Raw water level variation and magnetic field data at Honolulu, USA (HON).

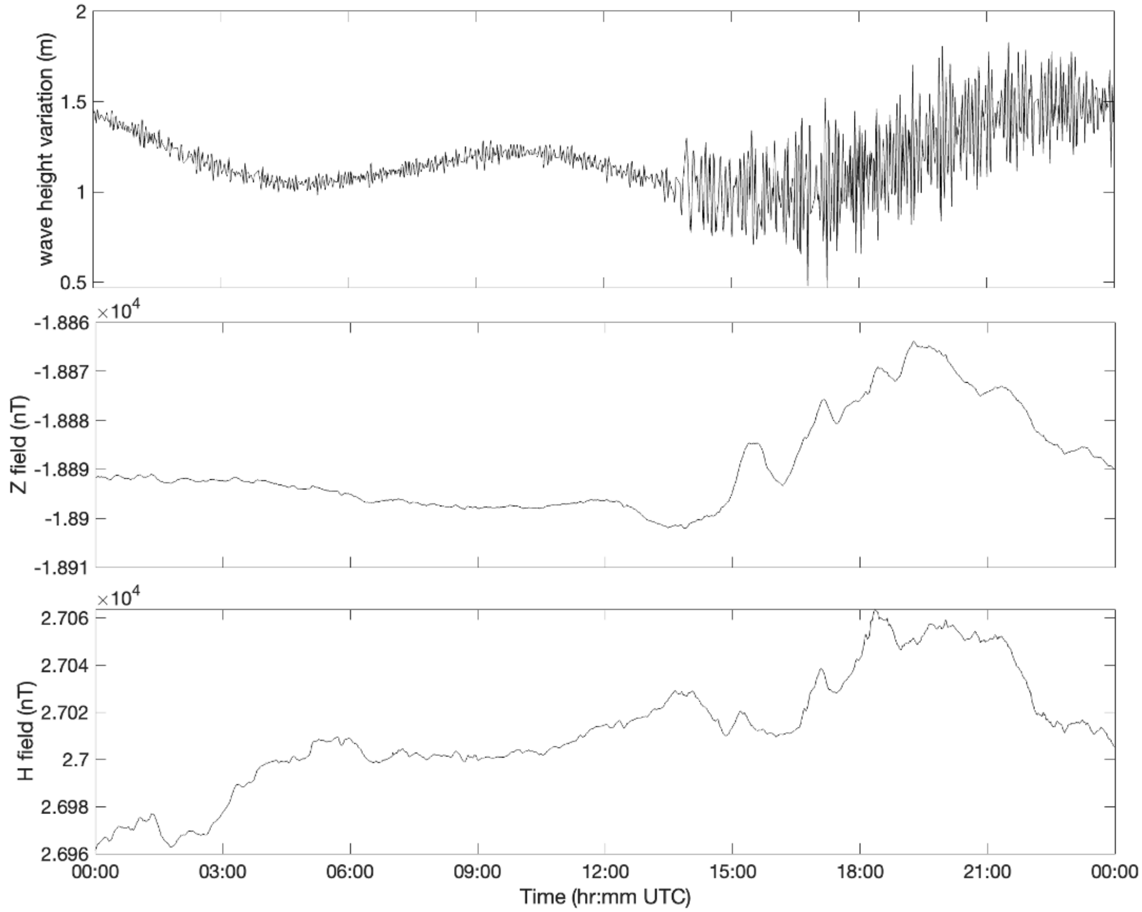

Figure S19. Raw water level variation and magnetic field data at Easter Island, Chile (IPM).

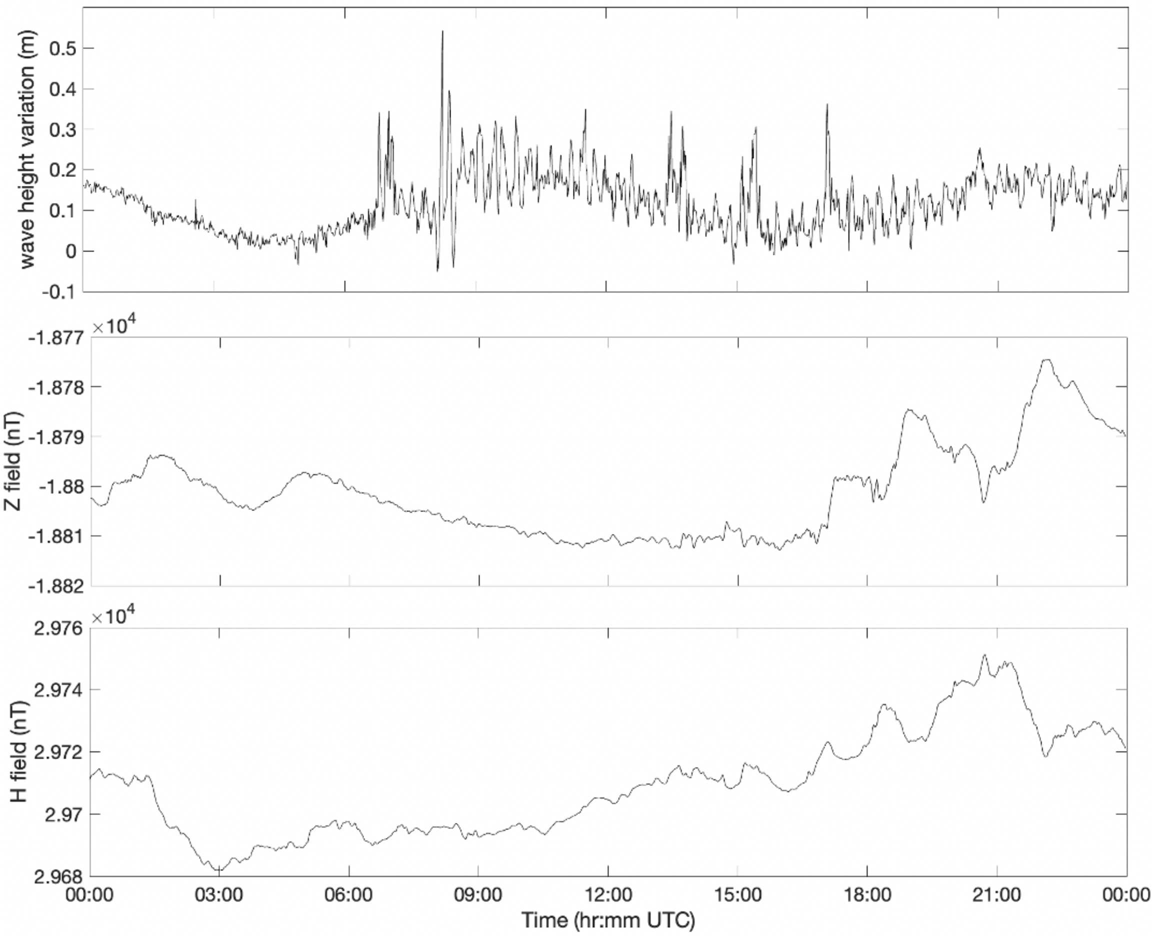

Figure S20. Raw water level variation and magnetic field data at Papeete, Tahiti, French Polynesia (PPT).

Cross-wavelet analysis spectrograms at Japanese observatories

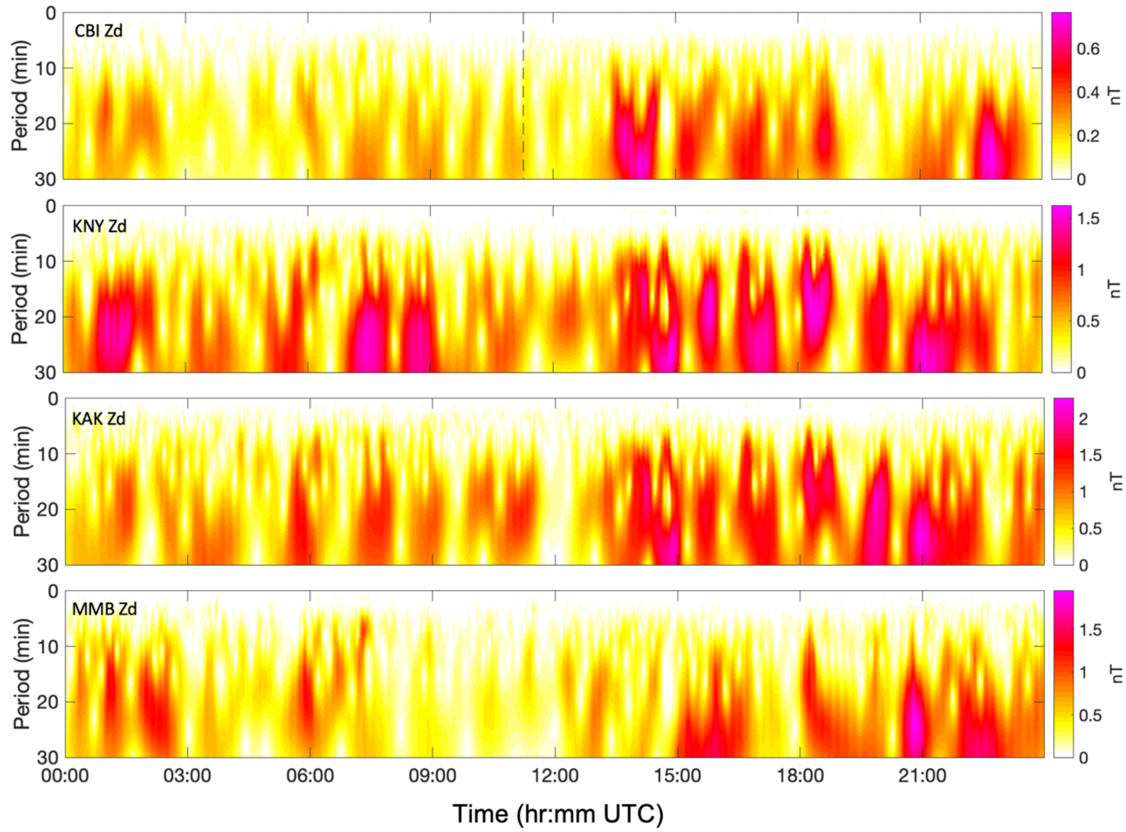

Figure S21. The cross-wavelet analysis results using T_{max}= 30 minutes at the Japanese observatories.

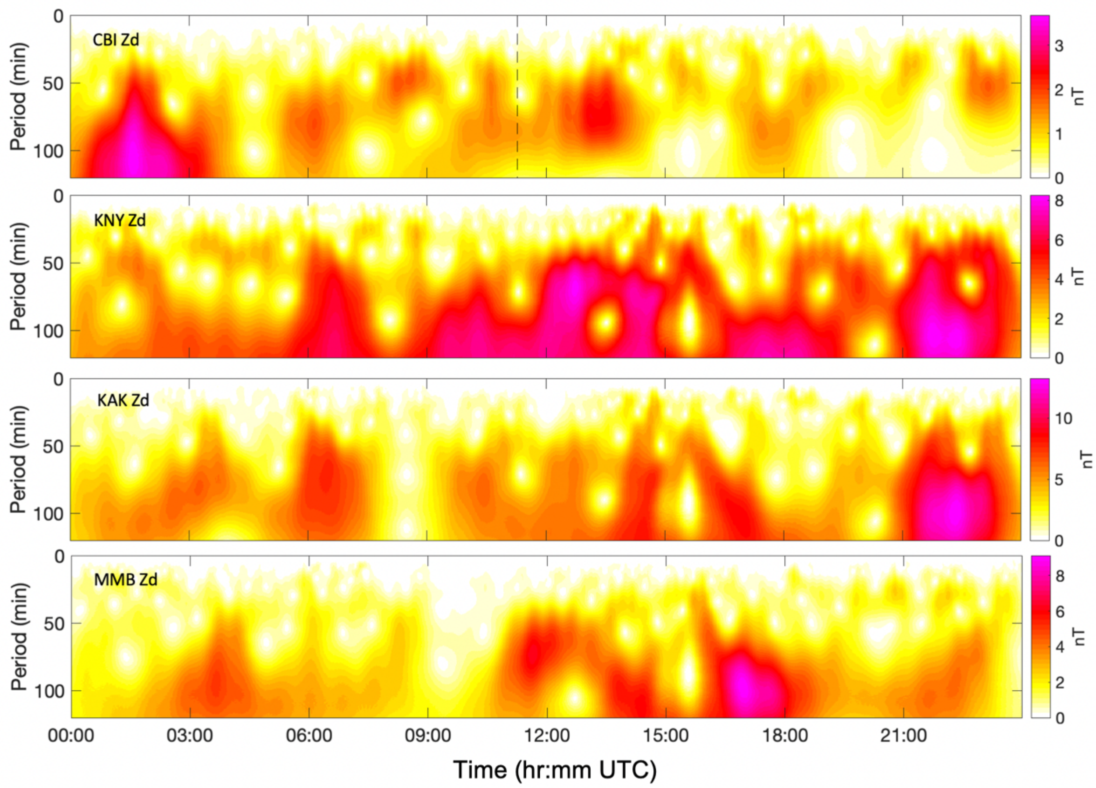

Figure S22. The cross-wavelet analysis results using T_{max}= 120 minutes the Japanese observatories.

Cross-wavelet analysis spectrograms at Oceania observatories

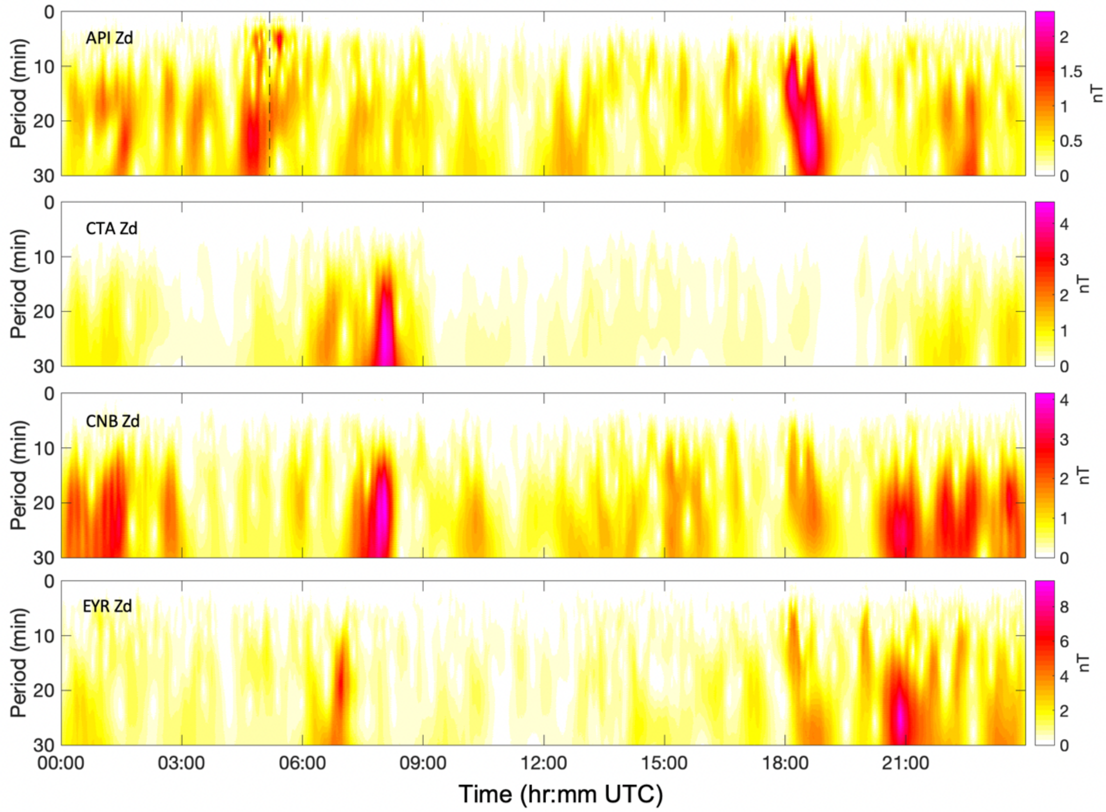

Figure S23. The cross-wavelet analysis results using T_{max}= 30 minutes the Oceania observatories. The vertical dashed line denotes the Western Samoa (API) water wave arrival determined from the water level data.

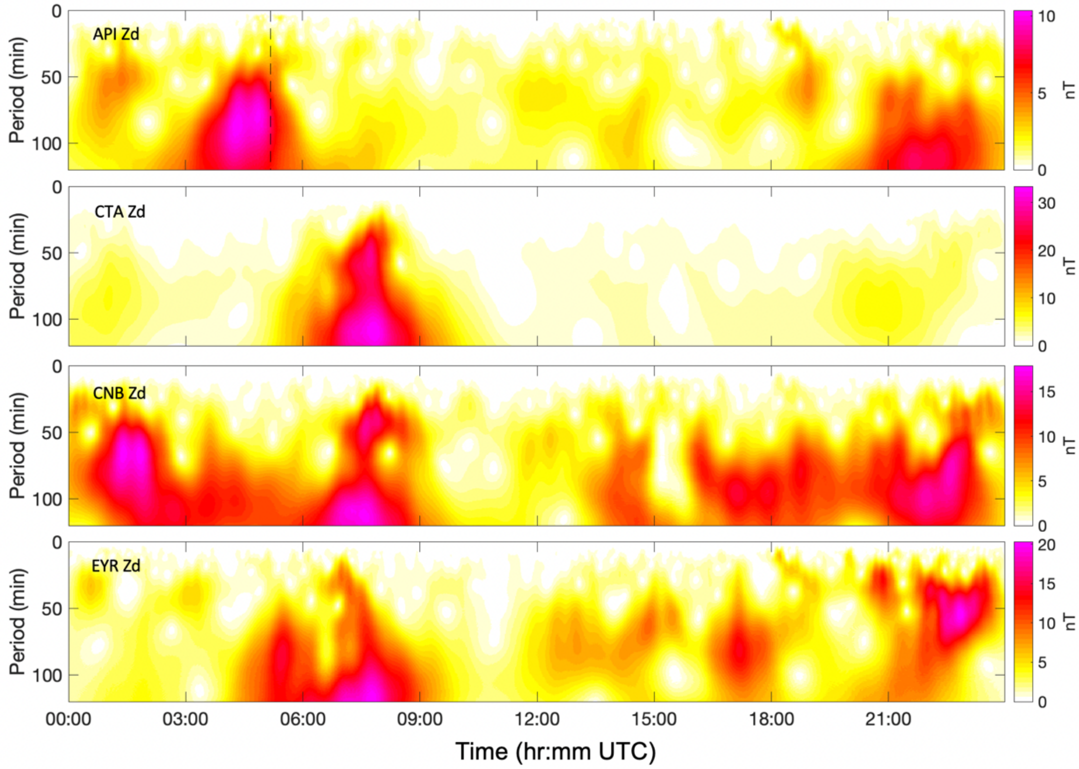

Figure S24. The cross-wavelet analysis results using T_{max}= 120 minutes the Oceania observatories. The vertical dashed line denotes the Western Samoa (API) water wave arrival determined from the water level data.

Cross-wavelet analysis spectrograms at mid-Pacific observatories

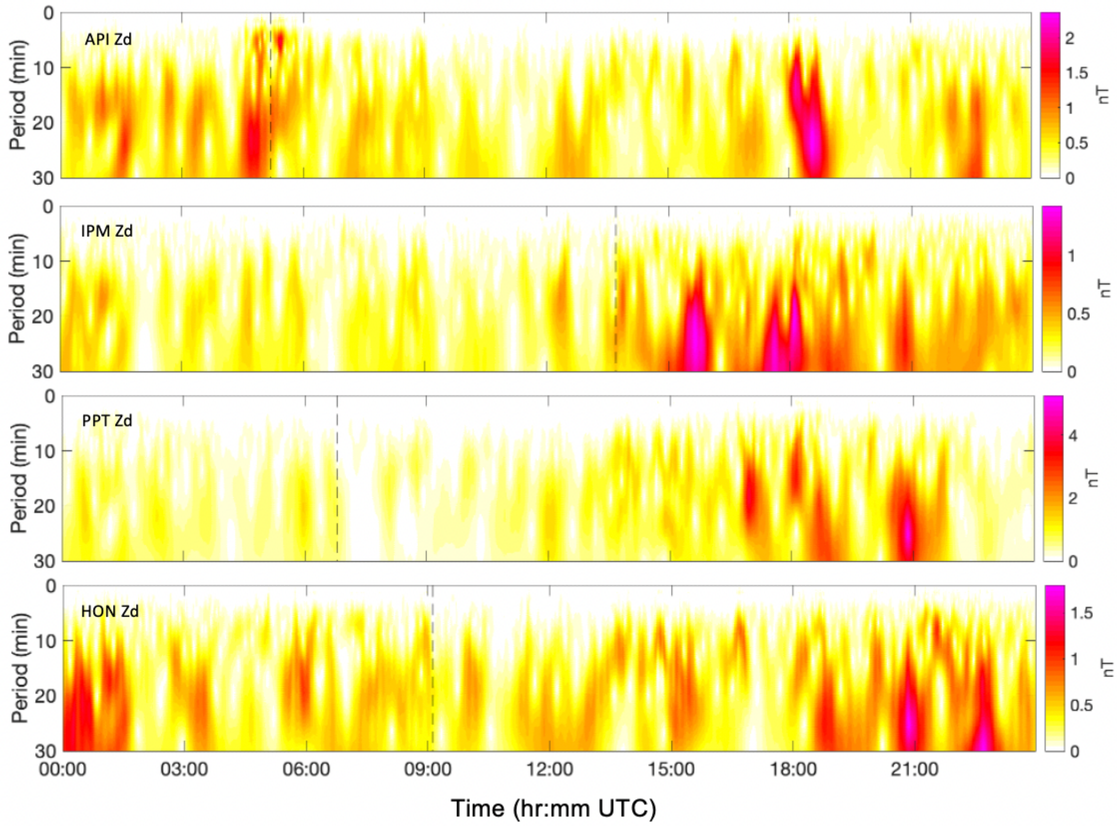

Figure S25. The cross-wavelet analysis results using T_{max}= 30 minutes the mid-Pacific observatories. The vertical dashed line denotes the water wave arrival determined from the water level data.

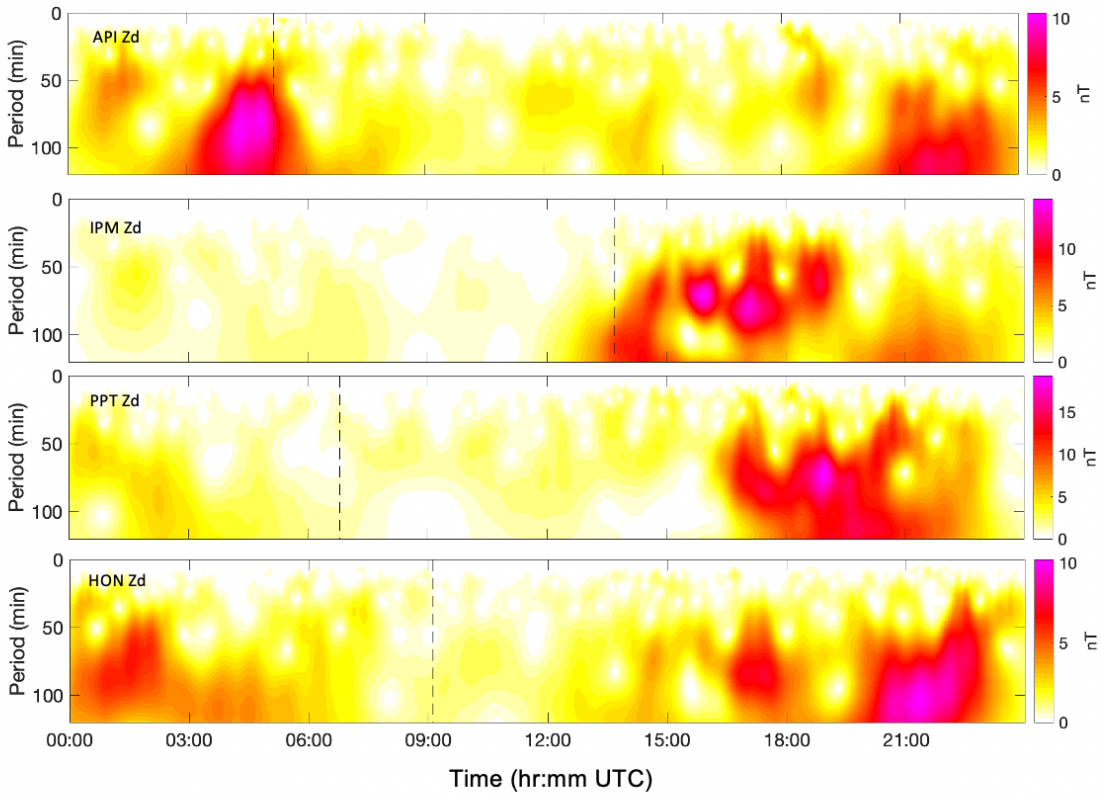

Figure S26. The cross-wavelet analysis results using T_{max}= 120 minutes the mid-Pacific observatories. The vertical dashed line denotes the water wave arrival determined from the water level data.